J Geod (2006) 80: 567–589
DOI 10.1007/s00190-006-0030-3

ORIGINAL ARTICLE

Pierre Bettinelli · Jean-Philippe Avouac
Mireille Flouzat · François Jouanne
Laurent Bollinger · Pascal Willis
Gyani Raja Chitrakar

Plate motion of India and interseismic strain in the Nepal Himalaya from GPS and DORIS measurements

Received: 4 November 2005 / Accepted: 27 January 2006 / Published online: 8 March 2006

Abstract We analyse geodetically estimated deformation across the Nepal Himalaya in order to determine the geodetic rate of shortening between Southern Tibet and India, previously proposed to range from 12 to 21 mm yr^{-1}. The dataset includes spirit-levelling data along a road going from the Indian to the Tibetan border across Central Nepal, data from the DORIS station on Everest, which has been analysed since 1993, GPS campaign measurements from surveys carried on between 1995 and 2001, as well as data from continuous GPS stations along a transect at the logitude of Kathmandu operated continuously since 1997. The GPS data were processed in International Terrestrial Reference Frame 2000 (ITRF2000), together with the data from 20 International GNSS Service (IGS) stations and then combined using quasi-observation combination analysis (QOCA). Finally, spatially complementary velocities at stations in Southern Tibet, initially determined in ITRF97, were expressed in ITRF2000. After analysing previous studies by different authors, we determined the pole of rotation of the Indian tectonic plate to be located in ITRF2000 at 51.409 ± 1.560° N and −10.915 ± 5.556°E, with an angular velocity of 0.483 ± 0.015°. Myr^{-1}. Internal deformation of India is found to be small, corresponding to less than about 2 mm yr^{-1} of baseline change between Southern India and the Himalayan piedmont. Based on an elastic dislocation model of interseismic strain and taking into account the uncertainty on India plate motion, the mean convergence rate across Central and Eastern Nepal is estimated to 19 ± 2.5 mm yr^{-1}, (at the 67% confidence level). The main himalayan thrust (MHT) fault was found to be locked from the surface to a depth of about 20 km over a width of about 115 km. In these regions, the model parameters are well constrained, thanks to the long and continuous time-series from the permanent GPS as well as DORIS data. Further west, a convergence rate of 13.4 ± 5 mm yr^{-1}, as well as a fault zone, locked over 150 km, are proposed. The slight discrepancy between the geologically estimated deformation rate of 21 ± 1.5 mm yr^{-1} and the 19 ± 2.5 mm yr^{-1} geodetic rate in Central and Eastern Nepal, as well as the lower geodetic rate in Western Nepal compared to Eastern Nepal, places bounds on possible temporal variations of the pattern and rate of strain in the period between large earthquakes in this region.

Keywords GPS · DORIS · Interseismic deformation · Tectonic plate convergence · Himalayas of Nepal

P. Bettinelli (✉) · M. Flouzat · L. Bollinger
Commissariat à l'Energie Atomique,
Laboratoire Détection et Géophysique,
91680 Bruyères-Le-Châtel, France
E-mail: pierre.bettinelli@cea.fr
E-mail: mireille.flouzat@cea.fr
E-mail: laurent.bollinger@cea.fr
Tel.: +33-169-266143
Fax: +33-169-267130

J.-P. Avouac
Tectonics Observatory, California Institute of Technology,
Pasadena, CA 91125, USA
E-mail: avouac@gps.caltech.edu

F. Jouanne
Laboratoire de Géodynamique des Chaînes Alpines,
Université de Savoie, Campus scientifique,
73376 Le Bourget du Lac Cedex, France
E-mail: francois.jouanne@univ-savoie.fr

P. Willis
Institut Géographique National, Direction Technique,
2 avenue Pasteur, BP 68, 94160 Saint-Mande, France

P. Willis
Jet Propulsion Laboratory, California Institute of Technology,
MS 238-600, 4800 Oak Grove Drive, Pasadena CA 91109, USA
E-mail: Pascal.R.Willis@jpl.nasa.gov

G. R. Chitrakar
Department of Mines and Geology, National Seismological Center,
Lainchaur, Kathmandu, Nepal.
E-mail: nscdmg@mos.com.np

1 Introduction

Crustal shortening in the Himalaya is known to absorb a large fraction of the plate convergence between India and Eurasia (Larson et al. 1999). This process has been responsible for

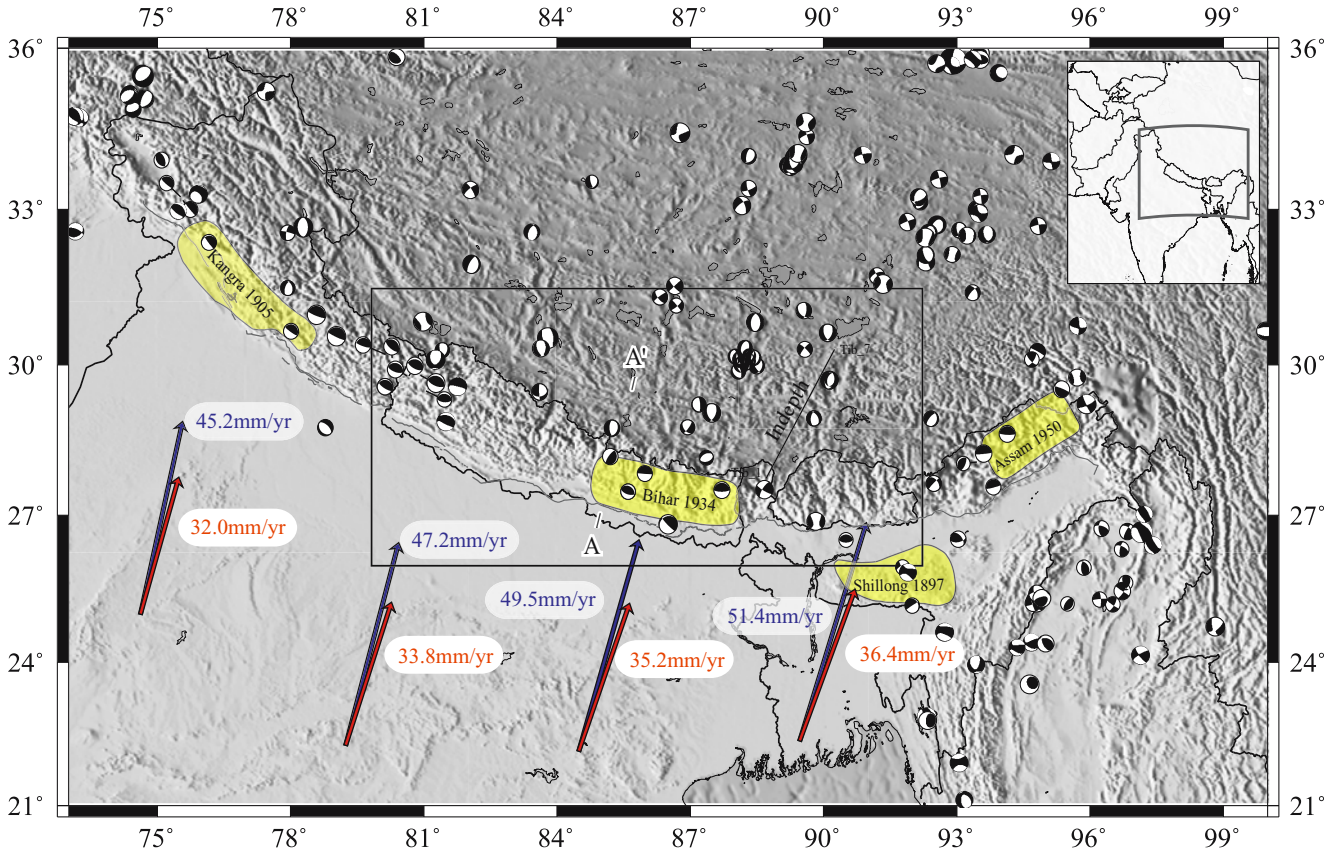

Fig. 1 Seismotectonic setting of the study area. Rupture area (*yellow area*) of major historical earthquakes along the Himalaya since 1897. Focal mechanisms from the Harvard Centroid-Moment Tensor (CMT) catalogue. *Blue arrows* show motion of India relative to Eurasia from the NUVEL-1A global plate motion model (Argus and Gordon 1991, De Mets et al. 1994). *Red arrows* show motion of India relative to Eurasia from the rotation pole determined in this study (26.45 ± 3.4°N, 13.99 ± 7.8°E, with an angular velocity of 0.354 ± 0.015° Myr^{-1}). AA' shows the location of cross-section in Fig. 2. The *box* shows the study area in Nepal

building the highest mountain range on Earth today and for recurrent large destructive earthquakes (Avouac 2003; Bilham et al. 1998) (Fig. 1). The geological shortening rate due to active thrust-faulting on the Main Himalayan Thrust (MHT) fault is estimated to be $21 \pm 1.5\,mm\,yr^{-1}$ on average over the Holocene period (Lavé and Avouac 2000). Geodetic measurements of crustal deformation bring information on the geometry of the locked portion of the MHT and would allow assessment of whether strain is stationary over the seismic cycle (Fig. 1).

In spite of efforts by a number of different groups (Table 1), the shortening rate across the Himalaya remains poorly constrained from geodetic measurements. There are huge discrepancies among the most recent estimates for the Nepal Himalaya. The various estimates, all determined from more or less the same GPS campaign data, were found to vary between $12\,mm\,yr^{-1}$ (Chen et al. 2004) and $19\,mm\,yr^{-1}$ (Jouanne et al. 2004), with the differences being much larger than the $1–2\,mm\,yr^{-1}$ (1σ) uncertainties ascribed to the various values reported in the literature (Table 1).

These estimates most probably underestimated the uncertainties due to ignorance of some source of errors. One main reason for the variability of these estimates is due to the poor control on the plate motion of India. Better geodetic constraints on Indian plate motion and on strain rates across the Himalaya would be a key to better understanding the dynamics of mountain-building and how deformation varies over the seismic cycle in the Himalaya.

For this purpose, we analysed all available GPS campaign data together with data from 4 continuous GPS stations (cGPS) (Flouzat et al. 2002) in the region, 1 DORIS station in the Nepal Himalaya at Everest (EVEB), 1 DORIS station on the Indian plate (COLA) and 19 International GNSS Service (IGS) stations, including IISC at Bengalore, which is the only one on the Indian plate. We chose to analyse the GPS and DORIS data independently and to express both results in ITRF2000 (Altamimi et al. 2002) so as to ensure compatibility.

Another approach would have been to combine the GPS solutions and the DORIS solutions obtained in a free-network (or loosely constrained) solution, as well as GPS–DORIS geodetic local ties with proper weighting, directly using the formal errors also provided by the Stations Installation and Maintenance Service (SIMB). Instead, we chose the independent approach so as to get rid of any systematic error in the geodetic local ties and also to prove that it is now possible to

Table 1 Summary of velocities across the Himalaya determined from previous studies and from this study

Article	Data	Region	Geometry of the creeping zone			Velocity	
			Depth (km)	Dip (°)	Strike	Amplitude (mm yr^{-1})	Azimuth
Jackson and Bilham (1994)	L	Np		3–6		13±8	
Bilham et al. (1997)	GPS	Np	20± 4	4± 4	Small circle N131@86E	20.5±2	Normal to the small circle
Jouanne et al. (1999)	GPS	NpW	17	9	N120	20.5	N180
Larson et al. (1999)	GPS+L	NpE	17.6	4.7	N105	20±1	
	GPS+L	Np	25	4.5	N120 (West)	21.3±1.6	
			14.9	3.4	N101 (East)	19.6±1.1	
Cattin and Avouac (2000)	GPS+L	NpC	–		N108	20	N198
Banerjee and Burgmann (2002)	GPS	InW	15	6	N133	14±1	N223
Boucher et al. (2004)	GPS+L	Np	17	5	Variable	19	Variable
Chen et al. (2004)	GPS	NpE				12.4 ± 0.4	
	GPS	NpW				17 ± 1	
	GPS	HiE				19 ± 1	
Jouanne et al. (2004)	GPS	Np	17–21	9–10	N117	19	
This study (2D solution)	GPS+L+cGPS	NpE+NpC	20	10	N113	16.3 ± 0.7	N023
	GPS	NpW	12	4.5	N120	13.4 ± 5	N030
This study (3D solution)	GPS+L+cGPS	NpE+NpC	20	10	Variable (cf.text)	19 ± 2.5	Variable (cf.text)
	GPS	NpW	12	4.5		13.4	

The second column indicates the data used in each study: *GPS* campaign GPS measurements; *L* vertical velocities determined from repeated levelling measurements along the road from Birganj to Kodari across Central Nepal; *cGPS* continuous GPS measurements. The third column indicates the area of interest in each study; *Np* whole of Nepal; *NpW* Western Nepal; *NpC* Central Nepal; *NpE* Eastern Nepal; *InW* Western India; *HiE* Eastern Himalaya

use direct geodetic products from a specific technique (station coordinates and velocities) with similar products from another technique (DORIS vs. GPS) for geophysical investigations. This compatibility is presently an important requirement in view of the current construction phase of the Global Geodetic Observing Service (GGOS, Beutler et al. 2005).

Hereafter, we first introduce the tectonic setting of the Nepal Himalaya. We then present the dataset, the processing strategy and geodetic results. Finally, we determine the Euler pole describing the motion of India in ITRF2000, and determine the shortening rate across the Himalayas from interseismic strain modelling.

2 Tectonic setting

The present-day structure of the Himalaya is characterised by a major thrust fault, the Main Himalayan Thrust (MHT) (e.g., Hauck et al. 1998) (Fig. 2). The MHT reaches the surface along the foothills, where it coincides with the Main Frontal Thrust (MFT) fault. To the north, it roots along a mid-crustal ramp into a shallow dipping zone of ductile shear that coincides with the mid-crustal reflector detected beneath the High Himalaya and Southern Tibet (Nelson et al. 1996). Deformation of Holocene terraces along the Bakeya and Bagmati rivers, south of Kathmandu, indicates 21 ± 1.5 mm yr^{-1} of shortening rate across the MFT (Fig. 2) (Lavé and Avouac 2000).

The deformation rates determined from geodetic measurements are all slower than the geologically estimated rates (Table 1). This discrepancy is puzzling and important to resolve since it might indicate that crustal strain is not stationary during the seismic cycle. This would be possible if the stress variations during the seismic cycle are comparable in magnitude to viscous stresses along the ductile portion of the MHT (Avouac 2003; Perfettini and Avouac 2004).

The plate convergence across the Himalaya has indeed produced recurrent large earthquakes with magnitude Mw > 8 that were documented either from historical accounts or paleoseismic studies (Bilham et al. 1998; Kumar et al. 2001; Lavé et al. 2005; Molnar and Pandey 1989). Four major earthquakes have, in particular, occurred over the first half of the last century (Fig. 1). These events have ruptured 250–300-km long segments of the arc with co-seismic slip estimated to around 5 m on average (Avouac et al. 2001).

Assuming a full seismic coupling of the upper MHT, such an event should have a recurrence period as short as 250 years (Avouac et al. 2001). The area between the 1934 and 1905 events (cf. Fig. 1) appears as a long-standing seismic gap, long enough for two M > 8 fault segments, or maybe an even larger magnitude event. The area west of Kathmandu thus stands as a potential location for the next large Himalayan earthquake. If interseismic strain is not stationary, there might be a significant difference between crustal strain across the Himalaya of Western and Eastern Nepal, possibly reflecting a more advanced stage in Western Nepal than in Eastern Nepal.

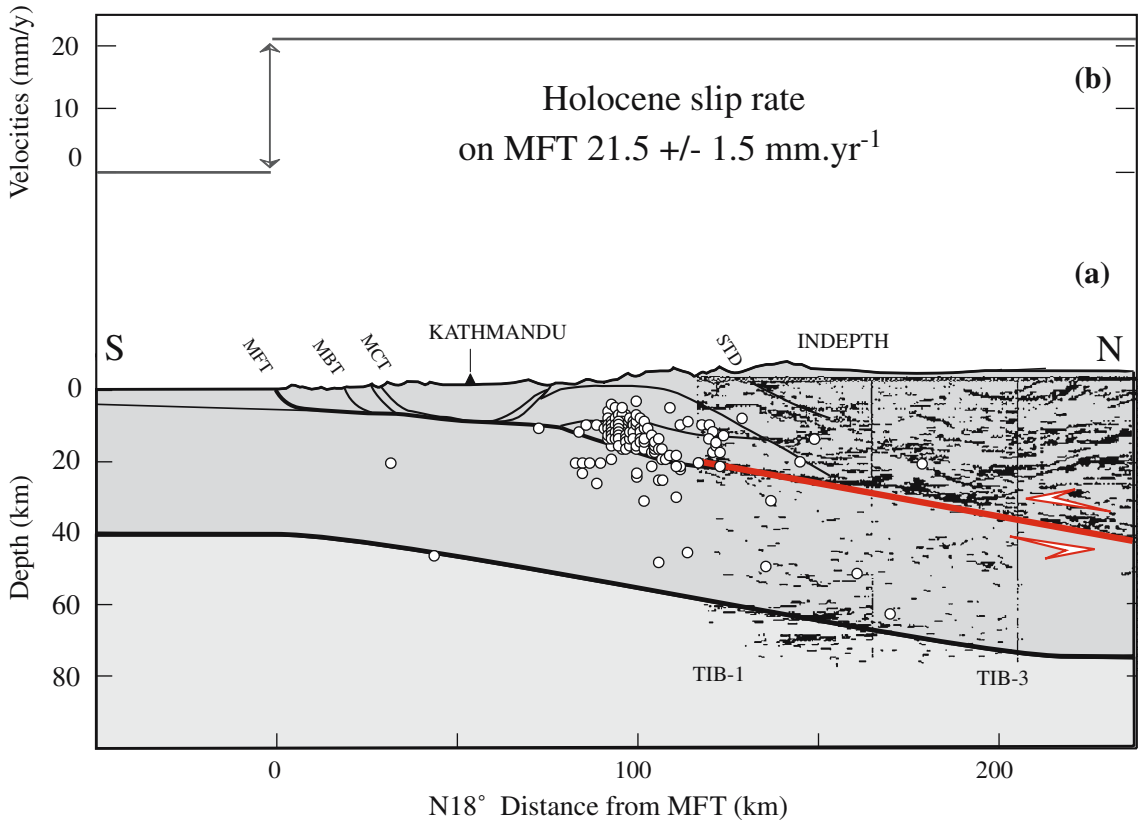

Fig. 2 **a** Structural cross-section across Central Nepal showing the major structures (*MFT* Main Frontal Thrust; *MBT* Main Boundary Thrust; *MCT* Main Central Thrust; *STD* Southern Tibet Detachment). Also shown are the *TIB-1* and *TIB-3* seismic sections of the INDEPTH profile (Hauck et al. 1998; Nelson et al. 1996; Zhao et al. 1993) (see their location in Fig. 1). All the thrust faults are inferred to root at depth in a sub-horizontal ductile shear zone that would correspond to the prominent mid-crustal reflector. The *red continuous line* shows the geometry of the creeping dislocation determined from the joint inversion of all geodetic data for Central and Eastern Nepal. The reported seismic events all have relatively well-constrained hypocentral depths thanks to the temporary deployment in 1995 of three 3-components seismic stations in addition to the permanent seismic network (Cattin and Avouac 2000). **b** Long-term geologically estimated velocities across Central Nepal, where the geological slip rate on the MFT is $21.5 \pm 1.5\,\mathrm{mm\,yr^{-1}}$ (Lavé and Avouac 2000)

3 GPS analysis and results

3.1 GPS network and observation history

Various GPS geodetic surveys were carried out in Nepal since 1991 as part of collaboration between the Department of Mines and Geology (DMG) of Nepal, CIRES (Colorado University, USA) and French laboratories under the Centre National de la Recherche Scientifique (CNRS) IDYL-HIM project (Commissariat à l'Energie Atomique/Laboratoire de Détection et Géophysique (CEA/LDG), Laboratoire de Géodynamique des Chaînes Alpines (LGCA)). The sites cover most of the Nepalese territory as shown in Fig. 3. Geodetic measurements were taken in 1995, 1997, 1998, 2000 and 2001 (Table 2).

In this study, we analyse all geodetic data collected between 1995 and 2001. We also include data from the three cGPS stations at Simra (SIMR), Daman (DAMA) and Gumba (GUMB), which have been operated since November 1997 by the CEA/LDG and the National Seismological Center in Kathmandu (DMG) (Figs. 3 and 4). We also included data from the station NAGA, near Nagarkot, deployed by CIRES in collaboration with the Survey of Nepal, which has been in operation sporadically between 1997 and 2001 (Figs. 3 and 4).

In order to directly determine station velocities in ITRF 2000 and then estimate velocities relative to the stable Indian plate, we also considered data from 19 additional regional IGS stations. These stations, including mainly IGS stations from South Asia, are listed in Table 3 and displayed in Fig. 5.

The locations of all sites used in this study are listed in Table 2, along with the date of observations, the number of sessions per point and the time span of the observation sessions. In 1995, both 12 h and 24 h sessions were conducted. In 1997, 1998, 1999, 2000 and 2001, 24 h sessions were mostly conducted. All measurements in 1995, 1997, 1998, 1999, 2000 and 2001 were made with dual-frequency geodetic receivers. GPS observations were recorded at a 30 s sampling rate using a cut-off elevation angle of 15° to reduce multipath effects and unmodelled tropospheric errors.

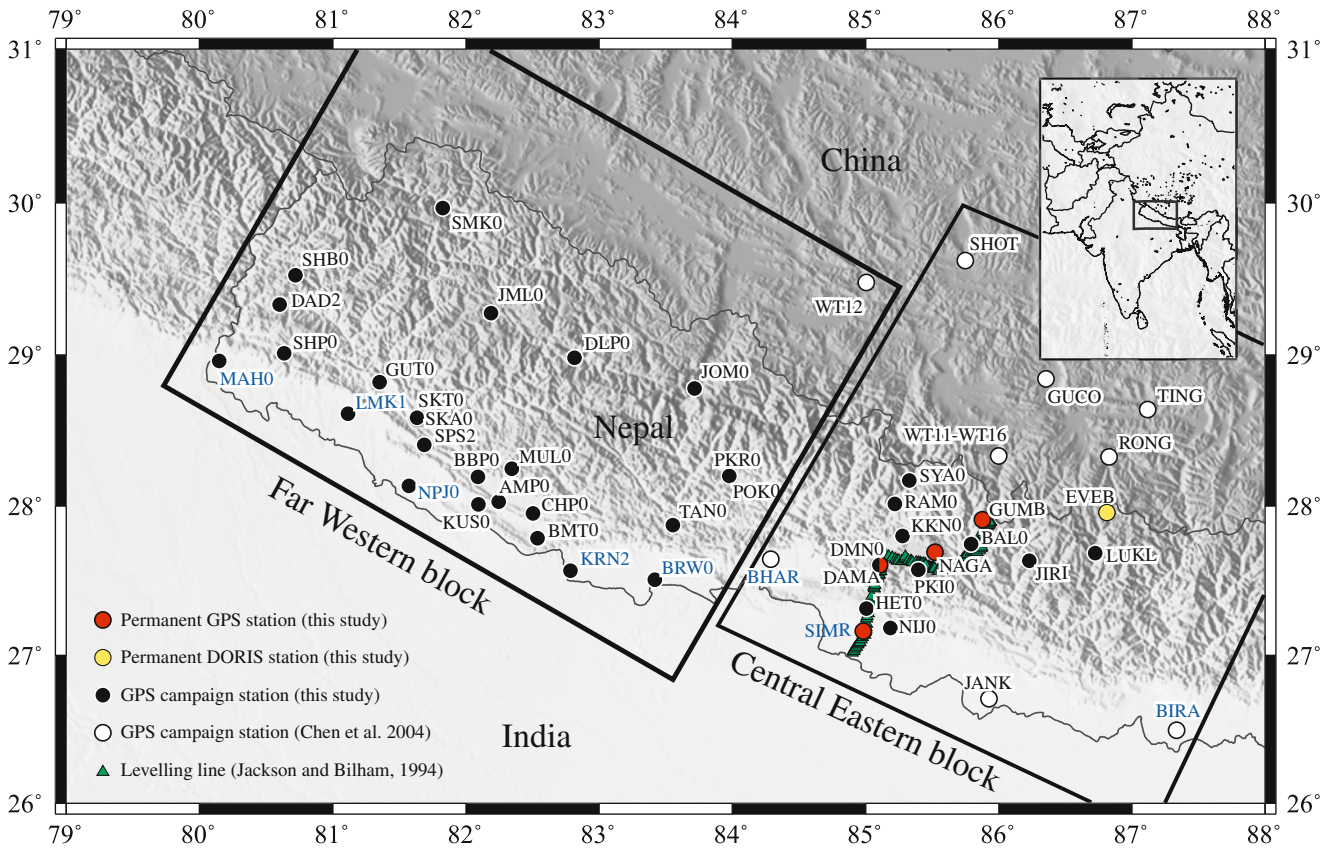

Fig. 3 Location of the cGPS (*red dots*), DORIS (*yellow dots*) and GPS campaign sites (*black dots* for this study; *white dots* from Chen et al. (2004)) analysed in this study. *Blue labels* indicate the stations used to determine the Indian plate motion The *two boxes* delimit the data sets used, respectively in the far Western and the Central-Eastern 2D modelling. Also shown is the location of the levelling line across Central Nepal (*green triangles*) (Jackson and Bilham 1994)

3.2 GPS data analysis – cGPS and campaigns

All available episodic and cGPS measurements were processed using the Bernese V4.2 software (Beutler et al. 2001). Results were obtained directly in the ITRF2000 reference frame, using IGS final precise orbits (Beutler et al. 1999), as recommended by Boucher et al. (2004), as well as IGS Earth rotation parameters and data from nearby IGS stations (Table 3).

We used the antenna phase center offsets and we computed phase center corrections using models provided by the IGS (National Geodetic Survey web site http://www.ngs.noaa.gov/). The heights of the defined reference point above the station mark on the ground were properly inserted in each file at the time of conversion of GPS data files from raw format to Receiver INdependent EXchange (RINEX) format.

Available nearby IGS permanent stations were included in the campaign data analysis. We computed a free network solution, assigning the following degrees of freedom to the IGS sites: $X = 0.02$ m; $Y = 0.02$ m; $Z = 1.0$ m, $V_x = 0.002\ \mathrm{m\,yr^{-1}}$; $V_y = 0.002\ \mathrm{m\,yr^{-1}}$; $Vz = 0.050\ \mathrm{m\,yr^{-1}}$. This enables us to express the coordinates of all campaign stations in a well-defined terrestrial reference frame (IGS0b) (Ray et al. 2004).

For the analysis of the first GPS data collected in 1995, we used the following strategy: an ionosphere-free analysis (Beutler et al. 2001) without ambiguity resolution in order to assess residuals, then a quasi-ionosphere-free (QIF) resolution strategy, which is a very powerful tool for resolving the ambiguities to integer values (Mervart 1995; Beutler et al. 2001). The continuous 24 h observation period permits a good determination of real ambiguity values using the QIF algorithm.

For the analysis of the most recent data (from 1997 to 2004) of better quality (due to improvements of receivers, antennas, precise code measurements, etc.), we were able to determine and fix the carrier-phase ambiguities using the following steps: an initial ionosphere-free analysis (same as for the 1995 data); resolution of the wide-lane ambiguities using the Melbourne–Wubbena linear combination depending on the quality of the code measurements (Melbourne 1985; Wubbena 1985); and finally a computation of the ionosphere-free solution introducing the resolved Melbourne–Wubbena linear combination ambiguities, which provides a reliable estimation of the station coordinates.

The troposphere-induced propagation delays were estimated from the observations every 2 h. Finally, for each day, we derived station coordinates in Software INdependant

Table 2 List of GPS sites processed in this study, with dates of observations and number of daily sessions

Station	Network	Latitude	Longitude	1995	1997	1998	2000	2001
AMP0*	IDYLHIM	28.0297	82.2474	2	–	4	4	–
BAL0*	LDG	27.7454	85.7945	2	–	3	–	–
BBP0*	IDYLHIM	28.1957	82.0937	3	–	4	–	–
BMT0*	IDYLHIM	27.7857	82.5398	2	–	2	4	–
BRW0*	CIRES+IDYLHIM	27.5073	83.4180	2	–	3	6	–
CHP0*	IDYLHIM	27.9509	82.5042	5	–	2	–	–
DAD2*	IDYLHIM	29.3342	80.6019	–	–	3	4	–
DAMA*	LDG	27.6081	85.1077	operated continuously since 1997 to 2004				
DLP0*	IDYLHIM	28.9828	82.8176	3	3	4	–	–
DMN0*	LDG	27.6081	85.1077	5	–	2	2	–
GUMB*	LDG	27.9098	85.8775	operated continuously since 1997 to 2004				
GUT0*	IDYLHIM	28.8237	81.3532	3	–	4	–	–
HET0*	LDG	27.3159	85.0078	3	–	3	3	–
JIRI	CIRES	27.6354	86.2304	9	–	–	–	3
JML0*	IDYLHIM	29.2772	82.1914	3	–	3	–	–
JOM0*	CIRES+IDYLHIM	28.7807	83.7179	12	–	2	–	–
KKN0*	LDG	27.8004	85.2791	5	–	12	17	–
KRN2*	IDYLHIM	27.5678	82.7848	–	–	2	6	–
KUS0*	IDYLHIM	28.0098	82.0952	3	–	–	4	–
LMK1*	IDYLHIM	28.6131	81.1158	2	–	4	–	–
LUKL	CIRES	27.6862	86.7262	4	–	–	4	–
MAH0*	CIRES+IDYLHIM	28.9632	80.1480	3	4	4	12	–
MUL0*	IDYLHIM	28.2494	82.3465	3	3	3	–	–
NAGA	CIRES	27.6927	85.5212	42	15	23	13	3
NIJ0*	LDG	27.1830	85.1866	2	–	3	–	–
NPJ0*	CIRES+IDYLHIM	28.1341	81.5747	6	16	6	5	–
PKI0*	LDG	27.5747	85.3982	4	–	13	12	–
PKR0*	IDYLHIM	28.1989	83.9776	1	–	2	3	–
POK0*	CIRES+IDYLHIM	28.1990	83.9777	4	–	9	2	–
RAM0*	LDG	28.0152	85.2221	1	–	2	5	–
SHB0*	IDYLHIM	29.5267	80.7214	3	–	4	4	–
SHP0*	IDYLHIM	29.0124	80.6364	1	4	3	4	–
SIMR*	LDG	27.1646	84.9844	operated continuously since 1997 to 2004				
SKA0*	IDYLHIM	28.5829	81.6343	–	10	19	10	–
SKT0*	CIRES+IDYLHIM	28.5858	81.6352	12	9	14	3	–
SMK0*	CIRES+IDYLHIM	29.9670	81.8265	10	5	4	–	–
SPS2*	IDYLHIM	28.4069	81.6906	–	3	4	3	–
SYA0*	LDG	28.1711	85.3293	2	–	2	3	–
TAN0*	CIRES+IDYLHIM	27.8738	83.5538	2	–	4	4	–

*All stations surveyed by LDG and IDYL-HIM teams, in collaboration with DMG

Table 3 List and location of IGS stations taken into account in the processing

IGS station	DOMES number	Longitude	Latitude	1995	1997	1998	2000	2001
BAHR	24901M002	50.608	26.209	–	X	X	X	X
BAKO	23101M002	106.849	−6.491	–	–	X	X	X
BJFS	21601M001	115.892	39.609	–	–	–	X	X
DGAR	30802M001	72.370	−7.270	–	X	X	X	–
IISC	22306M002	77.570	13.021	X	X	X	X	X
IRKT	12313M001	104.316	52.219	X	X	X	X	X
KIT3	12334M001	66.885	39.135	X	X	X	X	X
KSTU	12349M002	92.794	55.993	–	X	X	–	–
KUNM	21609M001	102.797	25.030	–	X	X	X	X
LHAS	21613M001	91.104	29.657	X	X	X	X	X
MALD	22901S001	73.526	4.189	–	–	–	X	X
NTUS	22601M001	103.680	1.346	–	X	X	X	X
POL2	12348M001	74.694	42.680	X	X	X	X	X
SEY1	39801M001	55.480	−4.674	X	–	–	X	X
SHAO	21605M002	121.200	31.100	X	–	–	X	X
TAIW	23601M001	121.537	25.021	X	–	–	–	–
URUM	21612M001	87.601	43.808	–	X	X	X	X
WUHN	21602M001	114.357	30.531	–	X	X	X	X
XIAN	21614M001	109.221	34.369	–	X	X	–	–

Cross station used; *minus* station not used. Also reported is the DOMES number of the stations (http://irtf.ensg.ign.fr/domes_desc.php)

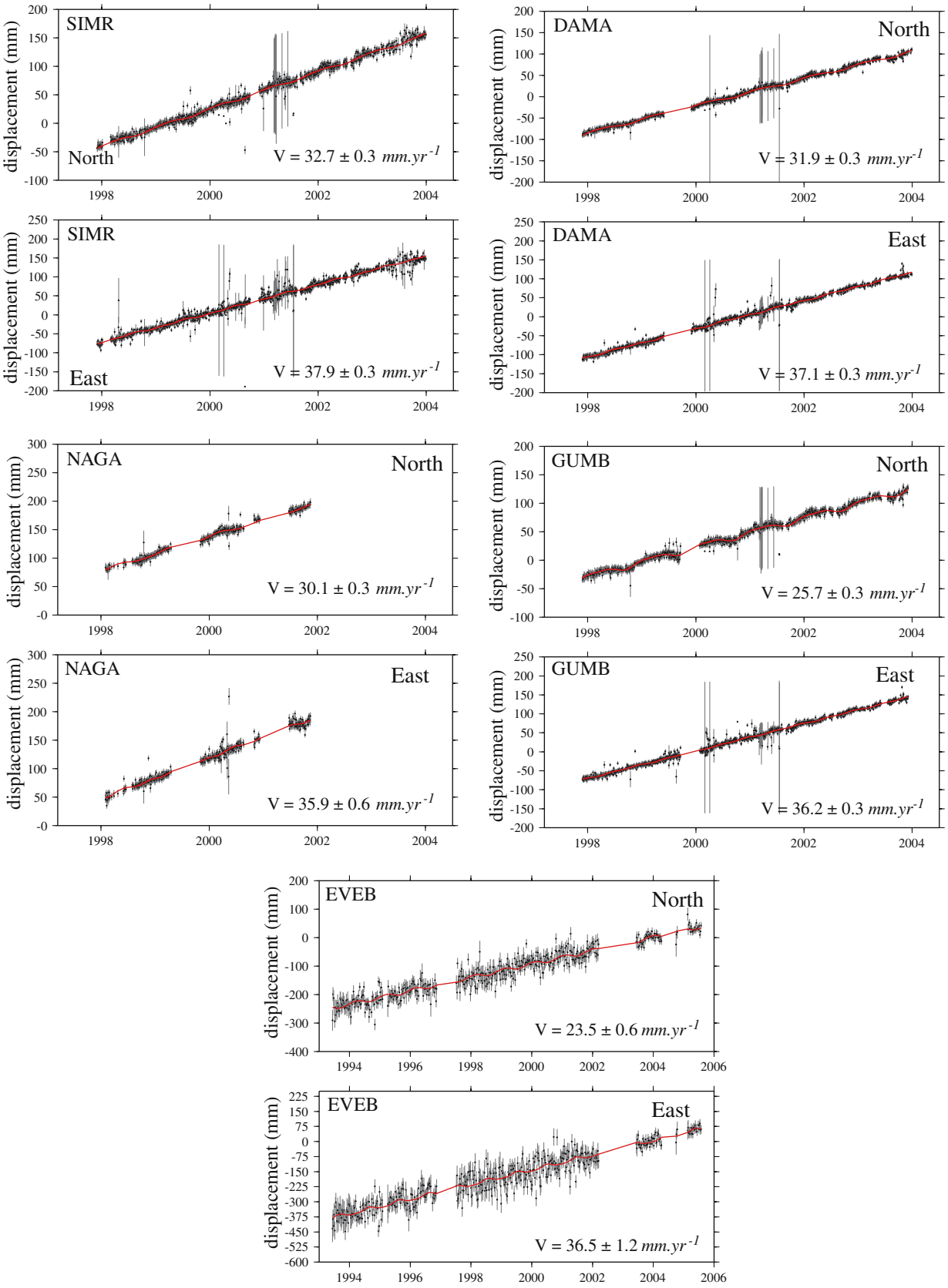

Fig. 4 Position as a function of time determined relative to ITRF2000 at cGPS stations (SIMR, DAMA, NAGA, GUMB) and at the DORIS station *EVEB*. The cGPS and DORIS data contain daily and weekly solutions, respectively. *Continuous lines* show best fitting models obtained from Eq. (1). The model parameters are listed in Table 6

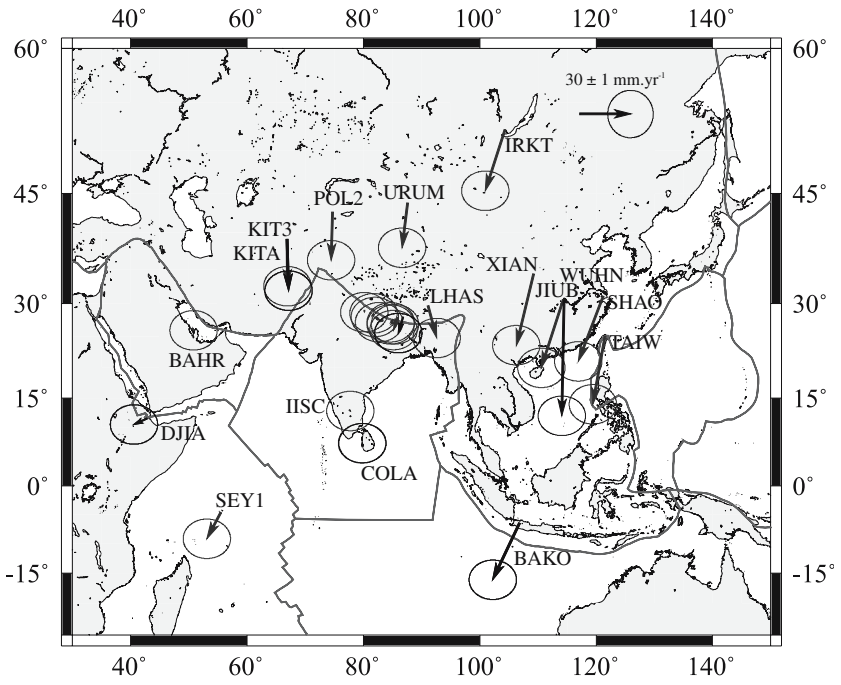

Fig. 5 Velocities relative to the Indian plate, as defined in this study (see the parameters in Table 7), determined at all cGPS and DORIS stations in Fig. 3. The DORIS station at *JIUB* is a new station and provides little data (i.e., since March 2004)

EXchange (SINEX) format (Blewitt et al. 1995), including a complete covariance information matrix. We used these independently processed daily solutions to estimate all GPS station velocities.

3.3 DORIS data analysis and results

We have analysed the DORIS data provided by the International DORIS Service (IDS) (Tavernier et al. 2005) using the GIPSY/OASIS II software (Webb and Zumberge 1995) at the Jet Propulsion Laboratory (JPL). Data were processed in a multi-satellite mode on a daily basis using the GGM01C GRACE-derived (Gravity Recovery And Climate Experiment) gravity field (Tapley et al. 2004; Willis and Heflin 2004).

We used all available DORIS data except that of Jason-1, whose data were not used at all due to an extreme sensitivity to radiation affecting the on-board DORIS clock when crossing the South Atlantic Anomaly (Willis et al. 2004, Lemoine and Biancale, submitted). We also excluded SPOT-4 data from 1998 for which a pre-processing error is present in the data file (Willis et al. 2006).

These daily solutions were combined into weekly solutions using a loose constraints technique. They correspond to the IGNWD04 free-network solutions available on line at the Crustal Dynamics Data Information System of the National Aeronautics and Space Administration (NASA/CDDIS) at ftp://cddis.gsfc.nasa.gov/pub/doris/products/sinex_series/ignwd.

In a second step, we combined all weekly DORIS solutions from January 1993 to May 2005 with additional SINEX matrices of all DORIS–DORIS geodetic local ties (using proper weighting), as provided by the IGN/SIMB (Fagard, 2005) who are in charge at the Institut Geographique National (IGN) of the installation and maintenance of the DORIS permanent tracking network. For stations at the same DORIS sites (i.e., successive occupations with different antennas), tight constraints were also added to the positions and velocities as SINEX files in the global adjustment.

Discontinuities in station coordinates (Willis and Ries 2005) were handled by introducing different station names. This allowed us to obtain a cumulative solution (positions and velocities of all DORIS stations estimated over the full period) in a free-network (Willis et al. 2005b). We then used a standard technique (Altamimi et al. 2002) to project the solution and finally transform it into ITRF2000. This solution is totally equivalent to the IGN04D02 cumulative solution, but it contains more DORIS data. We call it here IGN05D02P (preliminary) as it corresponds to the second cumulative solution computed in 2005, the first solution being the above free-network solution.

Figure 4 provides a synthesis of the currently available DORIS data for the Everest station (EVEB) at the NASA/CDDIS data centre. Even though the equipment has not been changed since June 1993 (same DORIS acronym), it can be seen that the station has suffered from several long periods without DORIS observations. This is not too surprising knowing the difficult weather conditions at this site and also the difficulty for the IGN/SIMB team to go there and make the necessary repairs. Table 4 provides a summary of previous determination of the Everest velocity in ITRF2000 using the EVEB DORIS data.

Table 4 Average velocities expressed in ITRF2000 and 1-σ uncertainties determined from the DORIS time-series at EVEB

Solution	N (mm yr^{-1})	E (mm yr^{-1})	U (mm yr^{-1})	Start	End	Data span (years)	
ITRF96	34.2 ± 12.2	51.3 ± 26.2	10.7 ± 18.8	JAN-93	JUL-97	4.5	(1)
ITRF97	23.2 ± 6.9	51.4 ± 9.1	10.7 ± 8.3	JAN-93	DEC-98	6.0	(1)
ITRF2000	22.9 ± 2.7	32.4 ± 5.4	3.2 ± 4.3	JAN-93	MAR-99	6.3	
LEGOS	31.4 ± 0.8	31.9 ± 2.1	-1.5 ± 1.1	JAN-93	DEC-96	4.0	(1)
IGN03D02	24.4 ± 0.6	35.6 ± 0.8	1.9 ± 0.3	JAN-93	DEC-03	11.0	
IGN04D02	23.1 ± 0.9	36.8 ± 1.0	1.4 ± 0.2	JAN-93	SEP-04	11.7	
IGN05D02P	23.3 ± 1.3	36.2 ± 1.9	1.6 ± 0.3	JAN-93	MAY-05	12.4	(2)

In the last column, (1) indicates that the 14-parameter transformation recommended by Altamimi et al. (2002) was used; (2) indicates that the discontinuity on January 1, 2001 was corrected. The ITRF96 and ITRF97 velocities are poorly determined because the amount of available DORIS data for these stations was very limited at that time. These variable velocities thus generate problems for the combination (Altamimi, personal communication, 2005)

In Table 4, three combined solutions using DORIS, as well other techniques such as GPS, VLBI and SLR are considered: ITRF96 (Sillard et al. 1998), ITRF97 (Boucher et al. 1999) and ITRF2000 (Altamimi et al. 2002). The DORIS-only solutions were also provided by the Laboratoire d'Etudes en Géophysique et Océanographie Spatiale (LEGOS) group (Soudarin et al. 1999; Crétaux et al. 1998) and by the IGN/JPL analysis group: IGN03D02 (Willis et al. 2005b), IGN04D02 (Willis and Heflin 2004), IGN05D02P (this analysis). Previous solutions provided by the above authors in ITRF96 or ITRF97 were transformed by us into ITRF2000 using the 14-parameter transformation recommended by Altamimi et al. (2002). All solutions are reported in Table 4.

For each solution in Table 4, we indicate the amount of DORIS data considered here by providing the start and end time of observation, as well as the duration between the two. It can be seen that the earlier solutions (ITRFs and LEGOS) are based on a smaller data span of DORIS observations, and provide larger formal errors. The first IGN/JPL solutions are very similar as they are based on the same time-series. Only the duration of observation is different. Formal errors should be larger in the case of the IGN05D02P solution, as a discontinuity was estimated for the EVEB station on January 1, 2001 as suggested by Laurent Soudarin on the IDS Analysis Forum at http://listes.cls.fr/wws/info/ids.analysis.forum.

It can be seen that this choice does not seem to affect the estimated velocity, which indicates that the discontinuity estimated at EVEB was probably small. The vector we estimated in this global adjustment was -9.0 mm in X, -0.3 mm in Y and 1.6 mm in Z. This is almost within the precision of the DORIS technique and we will not consider this discontinuity in the sequel.

The early ITRF solutions also show large vertical velocities (around 10 mm with extremely large formal error) (Table 4). The large formal errors could come from a down-weighting of the DORIS data (with respect to the other space-geodetic techniques). It can also be seen in Fig. 6 that these early ITRF solutions could not benefit from the 1997 to 2001 period, which corresponds to a large continuous amount of DORIS observations. The CIBB, DJIA, JIUB, KITA, COLA and EVEB solutions are illustrated on Fig. 5. The COLA and EVEB solutions are used hereafter, respectively to help constrain the Euler pole of India relative to ITRF2000 and the shortening rate through the Nepal Himalayas.

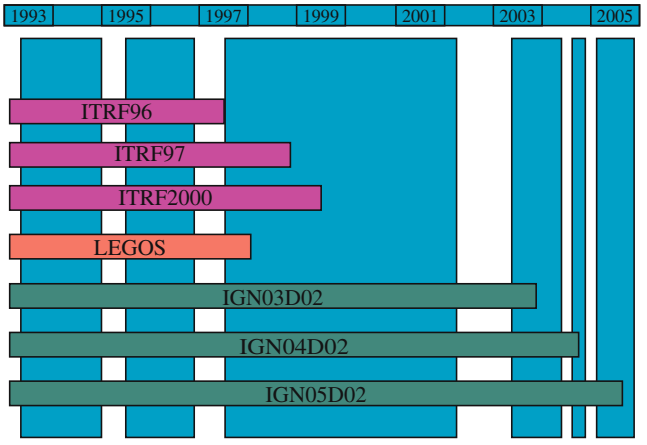

Fig. 6 Availability of DORIS data in recent DORIS terrestrial reference frames. *Vertical bars* correspond to the availability of actual DORIS data. *Horizontal bars* correspond to periods considered to estimate the different DORIS solutions by the different authors. Earlier solutions such as *ITRFs* and *LEGOS* were based on less data

3.4 Estimated velocities

We estimated GPS station positions and velocities using the quasi-observation combination analysis (QOCA) software (Dong et al. 1998; also see http://gipsy.jpl.nasa.gov/qoca/). Site velocities were estimated from the time-series of daily coordinates. The QOCA modelling of the time-series data was done through sequential Kalman filtering, allowing adjustment for global translation and rotation of each daily solution. Random-walk-style perturbations were allowed for some parameters whose errors were found to be correlated with time (e.g., Earth rotation parameters and the antenna heights at a few sites). For more details about the data analysis procedure and uncertainty estimation, refer to Shen et al. (2000) and http://gipsy.jpl.nasa.gov/qoca/. For the campaign GPS measurements, we estimate the secular velocity at each site from the best fitting linear function of time, adjusting the coordinates determined at each occupation. We use a weighted least squares criterion. All velocities and associated uncertainties are listed in Table 5.

The continuous GPS time-series show obvious seasonal variations (Fig. 4). Following Yoshioka et al. 2004, the average value ($b(t)$) and the uncertainty on the secular velocity

Table 5 Station velocities relative to ITRF2000 and to stable India with 1-σ uncertainties

			Velocity relative to ITRF2000 (mm yr^{-1})				Velocity relative to India (mm yr^{-1})			
Stations	Latitude	Longitude	North	σN	East	σE	North	σN	East	σE
AMP0_GPS*	28.0297	82.2474	34.3	0.9	36.7	0.9	0.9	0.9	−1.2	0.9
BAHR_GPS	26.2091	50.6081	28.3	1.6	31.4	1.4	−1.1	1.6	0.8	1.4
BAL0_GPS*	27.7454	85.7945	30.3	0.9	36.9	1.0	−3.0	0.9	−2.1	1.0
BBP0_GPS*	28.1957	82.0937	35.6	0.9	41.1	0.9	2.1	0.9	3.3	0.9
BMT0_GPS*	27.7857	82.5398	35.2	0.9	36.5	1.0	1.8	0.9	−1.5	1.0
BRW0_GPS*	27.5073	83.4180	32.1	0.9	35.8	1.0	−1.3	0.9	−2.6	1.0
CHP0_GPS*	27.9509	82.5042	35.8	0.9	39.8	1.0	2.3	0.9	1.8	1.0
DAD2_GPS*	29.3342	80.6019	30.0	0.8	36.4	0.9	−3.5	0.8	−0.6	0.9
DAMA_GPS*	27.6081	85.1077	31.9	0.3	37.1	0.3	−1.4	0.3	−1.7	0.3
DGAR_GPS	−7.2697	72.3702	17.6	3.4	53.1	3.9	−15.7	3.4	11.0	3.9
DLP0_GPS*	28.9828	82.8176	22.6	1.0	37.1	1.0	−10.8	1.0	−0.7	1.0
DMN0_GPS*	27.6081	85.1077	30.8	0.9	36.3	1.0	−2.5	0.9	−2.6	1.0
GUMB_GPS*	27.9098	85.8775	25.5	0.3	36.4	0.3	−7.8	0.3	−2.5	0.3
GUT0_GPS*	28.8237	81.3532	35.2	0.9	37.2	0.9	1.7	0.9	−0.2	0.9
HET0_GPS*	27.3159	85.0078	34.0	0.9	37.5	1.0	0.7	0.9	−1.4	1.0
IISC_GPS	13.0212	77.5704	32.7	1.4	41.4	1.6	−0.8	1.4	0.7	1.6
IRKT_GPS	52.2190	104.3162	−7.5	1.2	24.8	1.7	−37.8	1.2	−12.2	1.7
JIRI_GPS	27.6354	86.2304	25.2	1.0	37.6	1.1	−8.0	1.0	−1.5	1.1
JML0_GPS*	29.2772	82.1914	27.7	0.9	36.0	0.9	−5.7	0.9	−1.5	0.9
JOM0_GPS*	28.7807	83.7179	23.7	0.9	36.1	0.9	−9.6	0.9	−2.0	0.9
KIT3_GPS	39.1348	66.8854	3.6	0.9	28.3	0.9	−29.2	0.9	0.3	0.9
KKN0_GPS*	27.8004	85.2791	32.1	1.1	39.5	1.2	−1.2	1.1	0.7	1.2
KRN2_GPS*	27.5678	82.7848	35.1	0.9	35.3	1.0	1.7	0.9	−2.9	1.0
KUS0_GPS*	28.0098	82.0952	31.6	0.9	34.5	0.9	−1.8	0.9	−3.4	0.9
LHAS_GPS	29.6573	91.1040	12.8	1.0	45.3	1.0	−19.9	1.0	5.4	1.0
LMK1_GPS*	28.6131	81.1158	32.6	1.5	39.8	1.5	−0.9	1.5	2.3	1.5
LUKL_GPS	27.6862	86.7262	21.7	1.2	38.4	1.4	−11.5	1.2	−0.8	1.4
MAH0_GPS*	28.9632	80.1480	32.5	0.8	37.0	0.9	−1.0	0.8	0.0	0.9
MUL0_GPS*	28.2494	82.3465	35.0	0.9	37.6	0.9	1.5	0.9	−0.3	0.9
NAGA_GPS	27.6927	85.5212	30.1	0.3	35.9	0.6	−3.2	0.3	−3.0	0.6
NIJ0_GPS*	27.1830	85.1866	36.3	0.9	38.3	1.0	3.0	0.9	−0.6	1.0
NPJ0_GPS*	28.1341	81.5747	35.2	0.9	38.3	0.9	1.7	0.9	0.6	0.9
PKI0_GPS*	27.5747	85.3982	32.6	0.9	39.7	1.0	−0.7	0.9	0.8	1.0
PKR0_GPS*	28.1989	83.9776	30.9	0.9	40.4	1.0	−2.5	0.9	2.0	1.0
POK0_GPS*	28.1990	83.9777	34.4	0.9	38.0	1.0	1.0	0.9	−0.4	1.0
POL2_GPS	42.6798	74.6943	3.5	0.8	28.3	0.9	−29.9	0.8	−0.9	0.9
RAM0_GPS*	28.0152	85.2221	26.5	0.9	39.5	1.0	−6.8	0.9	0.8	1.0
SEY1_GPS	−4.6737	55.4794	14.5	3.0	34.4	3.6	−16.2	3.0	−8.5	3.6
SHAO_GPS	31.0996	121.2004	−15.6	1.7	32.1	3.0	−40.4	1.7	−15.5	3.0
SHB0_GPS*	29.5267	80.7214	28.8	0.8	36.0	0.9	−4.6	0.8	−1.0	0.9
SHP0_GPS*	29.0124	80.6364	34.9	0.9	37.3	0.9	1.4	0.9	0.2	0.9
SIMR_GPS*	27.1646	84.9844	32.7	0.3	37.9	0.3	−0.6	0.3	−1.0	0.3
SKA0_GPS*	28.5829	81.6343	31.9	0.9	34.9	0.9	−1.6	0.9	−2.7	0.9
SKT0_GPS*	28.5858	81.6352	31.4	0.9	36.7	0.9	−2.1	0.9	−0.9	0.9
SMK0_GPS*	29.9670	81.8265	24.1	0.8	35.6	0.9	−9.4	0.8	−1.5	0.9
SPS2_GPS*	28.4069	81.6906	34.4	0.9	38.3	0.9	1.0	0.9	0.7	0.9
SYA0_GPS*	28.1711	85.3293	26.4	1.0	38.1	1.0	−6.9	1.0	−0.6	1.0
TAIW_GPS	25.0213	121.5365	−17.6	3.2	40.0	2.2	−42.3	3.2	−7.6	2.2
TAN0_GPS*	27.8738	83.5538	35.3	0.9	37.7	1.0	1.9	0.9	−0.6	1.0
URUM_GPS	43.8079	87.6007	5.4	0.9	30.3	0.9	−27.7	0.9	−3.4	0.9
WUHN_GPS	30.5317	114.3573	−14.7	1.6	32.4	2.4	−42.1	1.6	−13.6	2.4
XIAN_GPS	34.3687	109.2215	−15.4	1.3	33.5	1.9	−44.3	1.3	−10.7	1.9
CICB_DORIS	−6.4906	106.8488	−5.5	1.4	23.3	2.0	−35.1	1.4	−16.7	2.0
CIBB_DORIS	−6.4906	106.8488	−5.5	1.4	23.3	2.0	−35.1	1.4	−16.7	2.0
COLA_DORIS	6.8920	79.8741	35.1	1.2	41.6	2.0	1.5	1.2	−0.3	2.0
COL1_DORIS	6.8920	79.8741	35.1	1.2	41.6	2.0	1.6	1.2	−0.1	2.0
EVE1_DORIS	27.9581	86.8131	23.5	0.6	36.5	1.2	−9.7	0.6	−2.7	1.2
EVEB_DORIS	27.9581	86.8131	23.3	1.3	36.2	1.9	−9.9	1.3	−2.9	1.9
DJIA_DORIS	11.5263	42.8466	23.3	1.0	29.0	2.0	−3.7	1.0	−8.1	2.0
DJIB_DORIS	11.5263	42.8466	23.3	1.0	29.0	2.0	−3.7	1.0	−8.1	2.0
JIUB_DORIS	30.5155	114.4911	−44.5	6.0	44.6	9.3	−71.8	6.0	−1.4	9.3
KITA_DORIS	39.1336	66.8848	0.8	1.2	29.0	1.7	−31.9	1.2	0.9	1.7
KITB_DORIS	39.1336	66.8848	0.8	1.2	29.0	1.7	−31.9	1.2	0.9	1.7
AIRP_CHEN	27.7000	85.2800	28.6	1.8	38.6	3.4	−4.7	1.8	−0.3	3.4
WT15_CHEN	27.4900	88.9100	22.0	1.9	40.8	2.8	−11.0	1.9	0.9	2.8

Table 5 (Contd.)

Stations	Latitude	Longitude	Velocity relative to ITRF2000 (mm yr^{-1})				Velocity relative to India (mm yr^{-1})			
			North	σN	East	σE	North	σN	East	σE
BALA_CHEN	29.7400	90.8000	12.9	1.8	45.7	2.2	−19.9	1.8	5.9	2.2
BHAR_CHEN	27.6700	84.4300	31.1	1.5	39.3	3.0	−2.2	1.5	0.7	3.0
BIRA_CHEN	26.4800	87.2600	32.4	1.9	41.6	3.2	−0.7	1.9	1.9	3.2
DAGZ_CHEN	29.6600	91.3600	10.9	1.8	46.3	2.1	−21.8	1.8	6.3	2.1
GNGB_CHEN	29.8800	93.2400	−0.3	2.5	56.1	3.2	−32.8	2.5	15.6	3.2
GGAR_CHEN	29.2800	90.9600	10.3	2.2	49.6	3.1	−22.5	2.2	9.6	3.1
GUCO_CHEN	28.7800	86.3400	18.7	1.8	43.3	3.2	−14.5	1.8	4.5	3.2
SHOT_CHEN	29.5900	85.7400	17.1	1.7	41.5	3.2	−16.2	1.7	3.1	3.2
JANK_CHEN	26.7100	85.9200	31.6	2.2	40.3	4.7	−1.6	2.2	1.1	4.7
JIAN_CHEN	28.9100	89.5700	17.3	1.6	42.4	2.1	−15.6	1.6	2.7	2.1
JIRI_CHEN	27.6400	86.2300	25.1	1.9	36.3	3.7	−8.1	1.9	−2.8	3.7
JOMO_CHEN	28.7800	83.7200	22.1	1.1	37.9	2.5	−11.3	1.1	−0.2	2.5
LHAS_CHEN	29.6600	91.1000	12.4	1.8	46.8	2.0	−20.4	1.8	6.9	2.0
LAZE_CHEN	29.1200	87.5800	20.0	1.4	42.8	2.3	−13.2	1.4	3.8	2.3
MAHE_CHEN	28.9600	80.1500	32.2	1.2	34.0	3.0	−1.3	1.2	−3.0	3.0
NAGA_CHEN	27.6900	85.5200	29.2	1.1	37.9	1.9	−4.0	1.1	−1.0	1.9
NEPA_CHEN	28.1300	81.5700	32.6	0.8	38.3	2.2	−0.9	0.8	0.6	2.2
WT11_CHEN	28.2900	86.0200	21.8	1.9	38.2	3.6	−11.5	1.9	−0.7	3.6
WT16_CHEN	28.3000	86.0200	19.2	1.4	40.6	2.4	−14.1	1.4	1.7	2.4
POKH_CHEN	28.2000	83.9800	28.3	1.3	37.4	2.7	−5.0	1.3	−0.9	2.7
RANJ_CHEN	28.0600	82.5700	29.0	1.5	37.7	3.1	−4.4	1.5	−0.3	3.1
RONG_CHEN	28.1900	86.8300	21.9	1.4	37.9	2.3	−11.3	1.4	−1.2	2.3
WT12_CHEN	29.4400	85.2100	20.2	1.2	34.1	2.3	−13.1	1.2	−4.3	2.3
SHIQ_CHEN	32.5100	80.1000	14.4	0.7	30.9	2.8	−19.1	0.7	−4.8	2.8
SIMA_CHEN	27.1600	84.9800	33.1	1.4	39.7	2.8	−0.3	1.4	0.7	2.8
SIMI_CHEN	29.9700	81.8300	18.9	1.1	34.4	2.7	−14.5	1.1	−2.7	2.7
SURK_CHEN	28.5900	81.6400	28.7	1.1	34.8	2.7	−4.8	1.1	−2.7	2.7
TANS_CHEN	27.8700	83.5500	27.9	1.5	37.7	3.1	−5.5	1.5	−0.6	3.1
TCOQ_CHEN	31.0200	85.1400	16.2	1.7	35.0	3.3	−17.1	1.7	−2.8	3.3
TING_CHEN	28.6300	87.1600	20.3	1.5	35.7	2.4	−12.9	1.5	−3.4	2.4
XIGA_CHEN	29.2500	88.8600	18.8	1.5	41.4	2.2	−14.2	1.5	2.0	2.2
WT15_CHEN	27.4900	88.9100	22.0	1.9	40.8	2.8	−11.0	1.9	0.9	2.8

The first part lists the GPS station velocities determined in this study from processing the raw data, the second part lists the DORIS station velocities obtained in this study from the combination in QOCA with all the GPS data, and the third part lists the GPS station velocities from stations in Southern Tibet obtained by converting the velocities determined by Chen et al. (2004) relative to ITRF97 to ITRF2000

* All stations surveyed by LDG and IDYL-HIM teams, in collaboration with DMG

at each station is computed with account for these seasonal variations by adjusting the time-series with the analytical function,

$$Y(t) = a + b(t) + c.\sin\left(\frac{2\pi t}{p}\right) + d.\cos\left(\frac{2\pi t}{p}\right) + e.\sin\left(\frac{4\pi t}{p}\right) + f.\cos\left(\frac{4\pi t}{p}\right). \quad (1)$$

The values of the different parameters in Eq. (1), obtained from adjusting the various time-series, are reported in Table 6 and the quality of fit is shown in Fig. 4. All velocities relative to ITRF2000 are reported in Table 5.

The uncertainties estimated from this procedure assume a white noise source of error. It has long been recognised that the main source of error in GPS time-series is in fact a flicker noise (Zhang et al. 1997). Williams et al. (2004, Figs. 4) show that flicker noise is a factor of 2–3 times higher than the corresponding white noise level. Based on that observation, we have increased our formal error estimated, assuming white noise, by a factor of 3. It should be noticed that the uncertainty on the secular velocities determined from the cGPS (5 years) and DORIS (7–12 years) stations is about three times better than those determined from campaign measurements.

We could not have access to the raw data from the campaign measurements carried out in Southern Tibet (Chen et al. 2004). In order to take some advantage of this dataset, however, we have used the velocities determined by these authors, which were given relative to ITRF97 (Boucher et al. 1999). These velocities were expressed relative to ITRF2000, using the transformation parameters produced by Altamimi et al. (2002) (see also http://itrf.ensg.ign.fr/). This transformation is described by the following equation:

$$\dot{X}_2 = \dot{X}_1 + \dot{T} + \dot{D}\,X_1 + \dot{R}\,X_1 \quad (2)$$

with

$$\dot{T}(\text{cm yr}^{-1}) = \begin{pmatrix} \dot{T}_1 \\ \dot{T}_2 \\ \dot{T}_3 \end{pmatrix} = \begin{pmatrix} 0.00 \\ -0.06 \\ -0.14 \end{pmatrix} \quad (3)$$

$$\dot{D}(\text{ppb yr}^{-1}) = 0.01 \quad (4)$$

Table 6 Coefficients of Eq. (1) used to fit the geodetic time-series with account for seasonal variations

	Coefficients							
	a	b	c	d	e	f	p(year)	p(days)
SIMR								
N	−65470.6	32.74790	1.87666	−1.19045	0.17678	0.38860	0.95003	346.76132
E	−75755.7	37.87990	−1.24903	−0.83845	0.27825	−1.25265	0.92498	337.61661
DAMA								
N	−63817.1	31.89800	1.88961	−2.29533	0.33145	−0.19133	0.97505	355.89216
E	−74190.6	37.07960	0.14850	−1.04260	−1.08334	−0.87599	1.00007	365.02555
NAGA								
N	−60124.1	30.13080	2.23975	1.42121	0.30220	−0.33042	0.92508	337.65530
E	−71749.1	35.93410	−1.35690	0.65572	−1.47554	−0.91557	1.02491	374.09215
GUMB								
N	−51460.8	25.74180	−4.43710	−1.07964	−0.73203	1.32306	0.99975	364.90693
E	−72299.4	36.15080	−0.70502	−0.24717	−1.09015	−0.56375	1.00005	365.01825
EVEB								
N	−47124.2	23.51580	−4.17672	4.60870	0.34308	0.31336	0.97522	355.95530
E	−73184.9	36.52200	−4.46430	6.82764	−1.93811	1.00231	0.97494	355.85420

Coefficients p(year) and p(days) correspond to the period expressed, respectively in years and in days

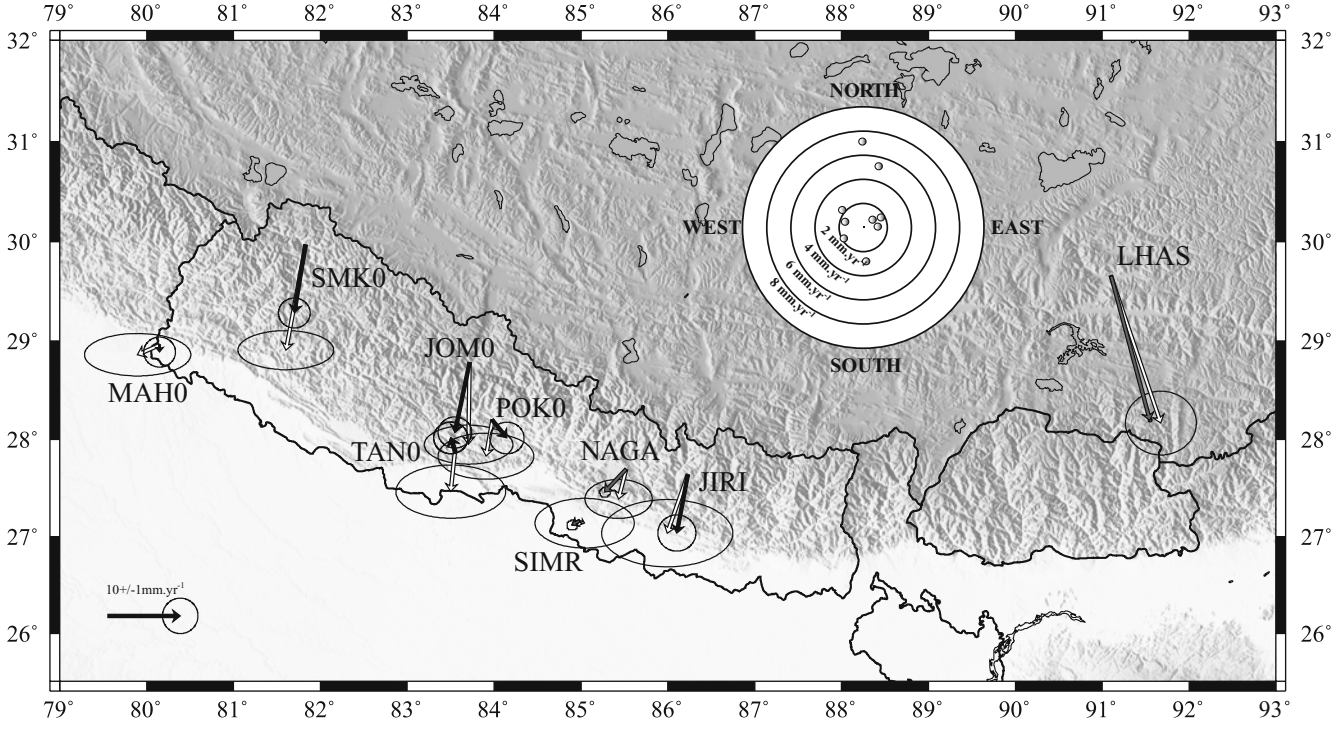

Fig. 7 Comparison of velocities relative to stable India as determined in this study and obtained by converting the velocities determined by Chen et al. (2004) relative to ITRF97 to ITRF2000. The differences between the two determinations are shown in the *azimuthal plot in the inset*

and

$$\dot{R}(0.001'' \,\mathrm{yr}^{-1}) = \begin{bmatrix} 0 & -\dot{R}_3 & \dot{R}_2 \\ \dot{R}_3 & 0 & -\dot{R}_1 \\ -\dot{R}_2 & \dot{R}_1 & 0 \end{bmatrix} = \begin{bmatrix} 0 & -0.02 & 0 \\ 0.02 & 0 & 0 \\ 0 & 0 & 0 \end{bmatrix} \quad (5)$$

in which X_i and $\dot{X}_i$ are, respectively the coordinate vector and its first time derivative.

In Fig. 7, we compare the velocities at nine common sites determined in our study with those obtained by Chen et al. (2004) after the above transformation. The discrepancies are less than about $2\,\mathrm{mm\,yr}^{-1}$ at six of the stations. We do not see any systematic errors in the geographic distribution of the differences between the two determinations, suggesting that there is no major reference frame issue when the two data sets are combined.

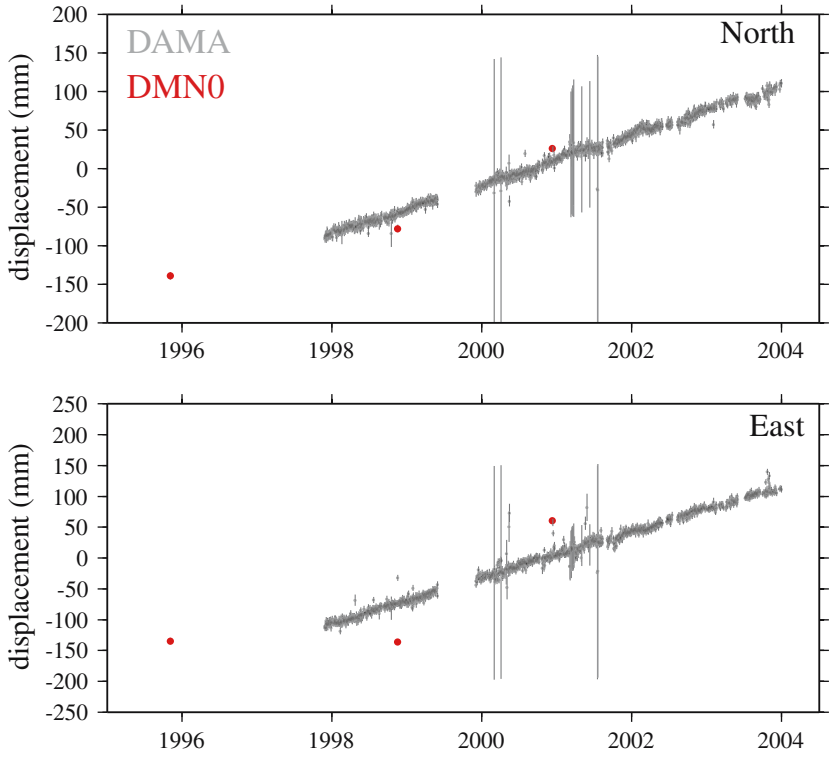

Fig. 8 Time-series comparison between the cGPS (DAMA, *grey dots*) and campaign measurements (DMN0, *red dots*) at the same site DAMAN (*red dots*)

The consistency between the campaign- and continuous-occupation solutions can be evaluated by comparing continuous time-series with campaign measurements at the same site. Figure 8 shows an example of the worst case, where the campaign measurements can be offset from the continuous time-series by more than 10 mm. The large errors on the campaign measurements are probably the results of short (less than 24 h) session lengths. As a result, the uncertainty on the velocity determined from the campaign measurements is typically three times larger than those derived from continuous measurements (Table 5). Although less accurate, the campaign data provide still some useful information on spatial distribution of strain.

4 Indian plate motion and velocity solutions

Euler poles and angular velocities describing the motion of most plates relative to ITRF97 and ITRF2000 have been already determined (Altamimi et al. 2002; Sella et al. 2002). However, it turns out that the motion of the Indian plate is relatively poorly constrained because previous determinations only used the sole IGS station on the Indian peninsular (IISC) and data from a relatively close ($< 5°$ spherical angle) continuous station (HYDE).

Recently, a better-constrained value, relative to ITRF2000 ($50.9 \pm 5.11°$N, $-12.1 \pm 0.61°$W and angular velocity $0.486 \pm 0.01°\,\mathrm{Myr}^{-1}$) was obtained by Socquet (2003) using IISC and HYDE together with our campaign measurements from stations in Southern Nepal: MAHE, NEPA, BHAR and SIMR (Fig. 3). We use the data from IISC, the campaign measurements at MAH0, NPJ0 (which are all south of the Himalayan foothills), the 1997–2004 time-series at the cGPS station SIMR and the 1993–2005 time-series at the DORIS station COLA in Columbo.

The best-fitting Euler pole is determined from minimising a reduced χ^2 criterion (Press et al. 1992), measuring the discrepancy between modelled (V_m) and observed (V_o) velocities, described by the following equation:

$$\chi^2 = \frac{1}{n}\sum_{i=1}^{i=n}\left(\frac{(V_\mathrm{o}^i - V_\mathrm{m}^i)}{\sigma^i}\right)^2, \tag{6}$$

where i refers to each data set.

Only horizontal velocities were taken into account in Eq. (6). We thus obtain an Euler pole describing the Indian plate motion relative to ITRF2000 (Table 7), located at $51.409 \pm 1.560°$N, $-10.915 \pm 5.556°$W, with an angular velocity of $0.483 \pm 0.015°\,\mathrm{Myr}^{-1}$. This determination is consistent with that of Socquet (2003).

The residual velocities are plotted in Figs. 5 and 9. Also shown in Fig. 9 are the residuals at four other stations located to the south of the Himalayan foothills (LMK1, KRN2, BRW0, BIRA). These stations were not considered in the determination of the pole of India to avoid putting too much weight on the data close to the Himalayan front, where interseismic strain might not be negligible. The residuals are generally less than about $2\,\mathrm{mm\,yr}^{-1}$ and they show no systematic pattern in terms of their geographic distribution.

Table 7 Summary of Euler poles describing the Indian plate motion relative to ITRF2000 and to Eurasia and the Eurasia plate motion relative to ITRF2000 determined from this and previous studies

Euler pole	Latitude(°)	Longitude(°)	Angular velocity(°/Ma)
India/ITRF2000 (this study)	51.409 ± 1.560	-10.915 ± 5.556	0.483 ± 0.015
India/ITRF2000 (Socquet 2003)	50.9 ± 5.11	-12.1 ± 0.61	0.486 ± 0.01
India/Eurasia (DeMets et al. 1994)	24.5 ± 1.8	17.7 ± 8.8	0.51 ± 0.06
India/Eurasia (Holt et al. 2000)	29.78	7.51	0.353 ± 0.024
India/Eurasia (Paul et al. 2001)	25.6 ± 1.0	11.1 ± 9.0	0.44 ± 0.026
India/Eurasia (Sella et al. 2002)	28.56 ± 1.1	11.62 ± 14.4	0.357 ± 0.033
India/Eurasia (this study)	26.45 ± 3.4	13.99 ± 7.8	0.354 ± 0.015
Eurasia/ITRF2000 (Altamimi et al. 2002)	57.965 ± 1.211	-99.374 ± 2.710	0.260 ± 0.005
Eurasia/ITRF2000 (SOPAC web site)	57.020 ± 0.15	-99.838 ± 0.58	0.258 ± 0.001

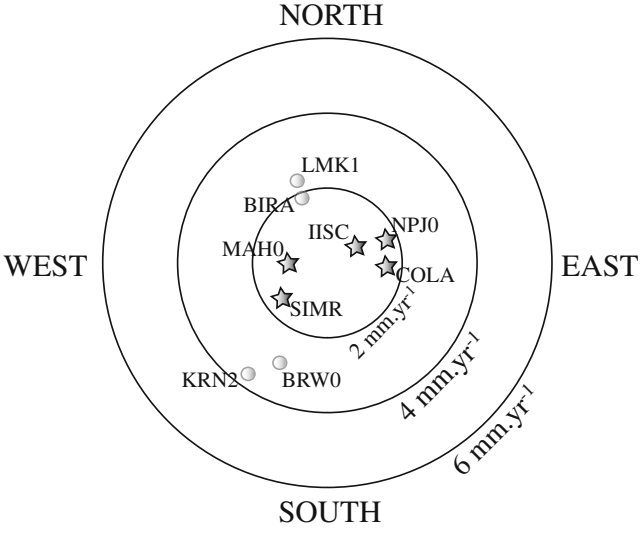

Fig. 9 Azimuthal plot of residual velocities at all stations presumed to be on the stable Indian plate, as determined in this study. *Stars* show stations which were used to determine the Euler pole of India in Table 7

The data set we consider is thus reasonably consistent with the hypothesis that they all belong to the same stable plate and that the effect of interseismic strain in the Himalaya is negligible among all these sites. All data relative to fixed India are reported in the Table 5. We have, in the same manner as earlier, calculated the Euler pole of the Indian plate compared to Eurasia (Table 7). For that, we transformed our ITRF2000 velocities into velocities relative to Eurasia, thanks to the Euler pole published by the Scripps Orbit and Permanent Array Center (SOPAC) (57.020 ± 0.15°N, -99.838 ± 0.58°E and angular velocity 0.258 ± 0.001° Myr^{-1}). This is similar to that published by Altamimi et al. (2002) (57.965 ± 1.211°N, -99.374 ± 2.710°E, 0.260 ± 0.005° Myr^{-1}), but presents a much smaller uncertainty.

We obtain an Euler pole describing the Indian plate motion relative to Eurasia, located at 26.45 ± 3.4°N, 13.99 ± 7.8°E, with an angular velocity of 0.354 ± 0.015°Myr^{-1}. Our Eurasia–India angular velocity predicts a station velocity of 34.4 mm yr^{-1} at IISC. We agree with earlier findings (Chen et al. 2000; Shen et al. 2000; Holt et al. 2000; Paul et al. 2001; Kreemer et al. 2000), suggesting that the Indian plate is moving slower than predicted by the NUVEL-1A global plate motion model (Argus and Gordon 1991; DeMets et al. 1994).

These studies show a range of velocity estimates (e.g., rates at IISC relative to Eurasia of 34.8, 41.9, 36, 43.7, and 34.3 mm yr^{-1}, respectively), but all are slower than the corresponding NUVEL-1A estimate of 47.8 mm yr^{-1} at IISC. Our velocity is comparable, though slightly smaller by 2% than previous geodetic estimates (Sella et al. 2002). It appears also to be about 30% slower than that predicted from NUVEL-1A global plate model.

5 Interseismic deformation in the Himalayas of Central Nepal

All the velocities were next determined relative to stable India as defined from the Euler pole obtained in Sect. 4 (Fig. 10). The estimated velocities, ranging from -3 to 3 mm yr^{-1} along the Himalayan foothills, increase gradually northwards across the Himalayan range, reaching 10–17 mm yr^{-1} in Southern Tibet. No detectable discontinuity of the velocity field is found across the MFT fault.

This shows that, over the 8-year time period covered by these data, the frontal part of the MHT has remained locked, as already argued in a number of previous studies in Nepal (e.g., Bilham et al. 1997; Cattin and Avouac 2000; Jouanne et al. 1999; Larson et al. 1999) and in the North-Western Himalaya (Banerjee and Burgmann 2002).

In Fig. 11, we compare the observed velocities with the prediction of the model of interseismic straining that was proposed by Boucher et al. 2004. This model assumes that the MHT is locked from the surface to some depth below the front of the high range. The location of the down-dip end of the locked fault zone was determined from the seismicity pattern based on the rationale of Cattin and Avouac 2000, who demonstrated that seismicity is triggered by a Coulomb stress increase at the tip of the creeping portion of the MHT.

In that model, the convergence rate is assumed to be 19 mm yr^{-1} (Boucher et al. 2004, Table 1), similar to the long-term geologically estimated rate. The model predicts a reasonable fit to our new results, although the assumed convergence rate seems too high. We therefore search for the best slip rate solution across Eastern and Central Nepal, keeping all geometric properties the same in the model. The best-fitting slip rate is determined to be 15.7 ± 5 mm yr^{-1} (Table 8). It should be noticed here that the error estimate does not

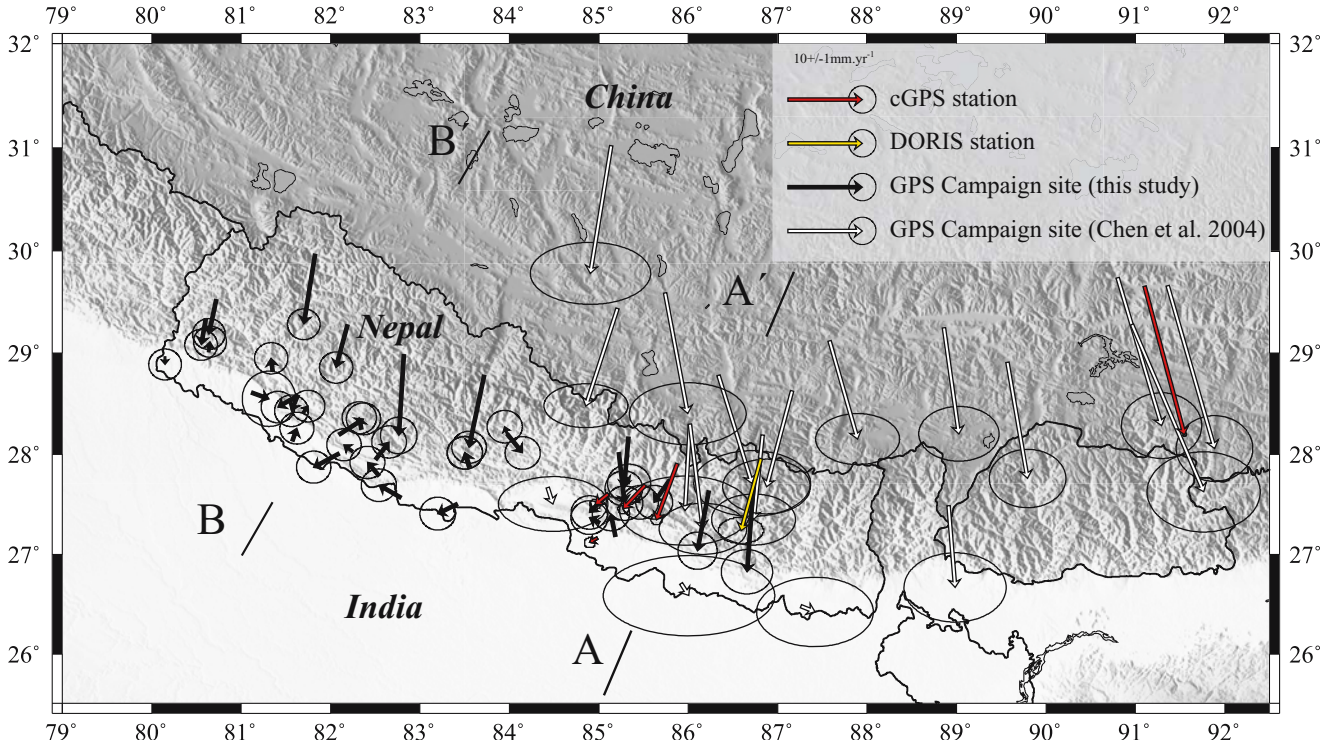

Fig. 10 Velocities at all sites relative to stable India. *Red, yellow, and black arrows* represent, respectively, the velocities determined in this study at the cGPS stations, the DORIS station, and the campaign stations in Nepal. The *white arrows* show the velocities in Southern Tibet and Nepal obtained by converting the velocities determined by Chen et al. (2004) relative to ITRF97 and ITRF2000. AA' and BB' show location of profiles across Central-Eastern Nepal and Western Nepal shown in Figs. 12 and 13

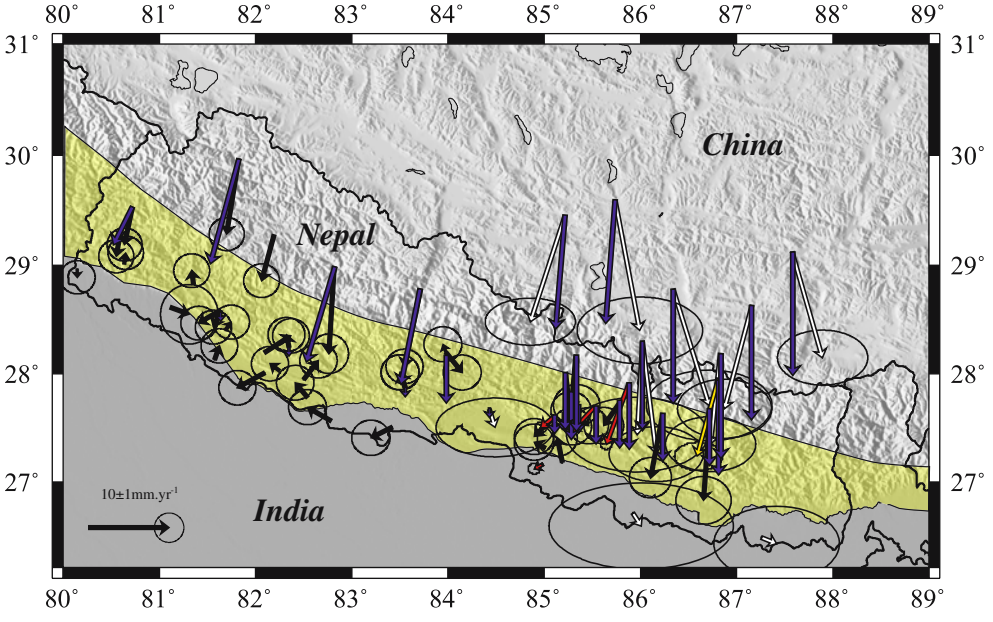

Fig. 11 Observed velocities relative to stable India (same colour code as in Fig. 10), as determined in this study, and velocities predicted from a 3D dislocation model (Boucher et al. 2004) (*blue arrows*). The *yellow area* shows the geometry of the locked fault zone of the MHT assumed in this model

Table 8 Convergence rates, with 1-σ uncertainty, across Eastern Nepal and Western Nepal determined from a model of interseismic strain with the same fault geometry and slip azimuth as in Bollinger et al. (2004)

	Block east (Boucher et al. 2004)	Block west (Boucher et al. 2004)
V ($mm\,yr^{-1}$)	15.73 ± 5	12.5 ± 6
χ^2 on the north component	1.47	4.25
χ^2 on the east component	1.25	2.75
χ^2 on both components	1.37	3.5

The convergence rate was adjusted by minimising the reduced χ^2 criterion

Table 9 Parameters of the best fitting 2D dislocation models (Singh and Rani 1993) for Eastern and Western Nepal, obtained by minimising the reduced χ^2 criterion

	Eastern Nepal			Western Nepal
	Inversion of horizontal data	Inversion of vertical data	Inversion of horizontal and vertical data	Inversion of horizontal data
V ($mm\,yr^{-1}$)	16.3 ± 0.7	12.1 ± 0.4	16.2 ± 0.8	13.4 ± 5
Dip(°)	10.3	11.5	10.3	4.5
Downdip end (km)	115	104	112	151
Depth (km)	20.9	21	20.4	12.1
χ^2 on the GPS Data (G)	**1.87**	6.67	1.92	5.88
χ^2 on the Leveling Data (L)	2195.39	**0.88**	0.94	–
χ^2 on both G and L	1153.2	2.35	**1.08**	–

Bold values indicate the χ^2 criterion that was minimised to derive the model considered. Other values are listed for comparison

account for the uncertainty on the model geometry or on the plate motion of India.

In order to find a local (i.e., Eastern or Western Nepal) best-fitting slip rate with as few geometrical assumptions as possible, such as a free-locked fault zone location or a free-creeping zone dip and depth, we modelled the data using a simpler 2D elastic dislocation model. Following most previous investigations (e.g., Bilham et al. 1997), we model interseismic strain as due to slip along a creeping dislocation embedded in an elastic half-space. Although this modelling approach is questionable, it has been shown to be a reasonable approximation when compared to mechanical models that account for the variations with depth of rheological properties, as well as to the effect of erosion and sedimentation on crustal deformation (Vergne et al. 2001).

We use the analytical solution for a pure dip-slip fault in an elastic half space (Singh and Rani 1993). To account for the uncertainty on the plate motion of India, the model is parameterised in terms of the coordinates of the Euler Pole of India relative to ITRF2000, the geometry of the locked fault zone (assumed fixed relative to India) and the slip-rate. We then minimise the χ^2 (Eq. 6) taking into account the velocities relative to ITRF2000 of all sites on the Indian plate and across the Nepal Himalaya (listed in Table 5). This inversion procedure allows another solution for the plate motion of India. The various solutions described hereafter all yield a solution for the Euler pole of India very close to that proposed at the end of Sect. 4 with generally slightly smaller uncertainties. Hereafter, we will focus on the results on the locked fault zone geometry and slip rates.

Because of the arcuate shape of the Himalayan arc and because of possible differences between Western and Eastern Nepal, we considered two sections. Only the component of the velocity parallel to the dip-slip motion is considered in this analysis (i.e., horizontal data). In Central and Eastern Nepal, projecting the geodetic data along a N23°E section, an azimuth normal to the midcrustal microseismic cluster stretch, the solution best fitting all horizontal GPS data yields a slip rate on the MHT of $16.3 \pm 0.7\,mm\,yr^{-1}$, with a relatively good fit to the data corresponding to a reduced χ^2 of 1.87 (Table 9). It should be noticed that this 2D model assumes that all displacements are parallel to the N23°E azimuth of convergence. If the velocity components in the N113°E azimuth are taken into account, the reduced χ^2 increases to 4.00.

The 2D approximation turns out to be a poor approximation. This model was also compared with uplift rates determined from the comparison of spirit levelling data across Central Nepal (Jackson and Bilham 1994). These data show uplift rates relative to the first point in the lowland. The fit is poor, yielding a reduced χ^2 on the vertical data of about 2,200 (Table 9). The main reason for the poor fit is that the horizontal velocities poorly constrain the position of the down-dip end of the locked fault zone.

We also determined the best-fitting solution obtained from only the vertical data. One unknown parameter is the absolute elevation change of the levelling first point, which we need to solve for, as suggested by Gahalaut and Chander (1997). A good fit (χ^2 of 0.9) is obtained for a slip rate of $12.1 \pm 0.4\,mm\,yr^{-1}$; the best fitting uplift rate at the first point is then $0.9\,mm\,yr^{-1}$. The dip-angle of the creeping dislocation is not affected much, still of the order of 10°, but the down-dip end of the locked fault zone is shifted southward by 11 km.

When both data sets are considered simultaneously, we obtain a good general fit to the data with a χ^2 of 1.08. This shows that the two data sets are reasonably consistent and

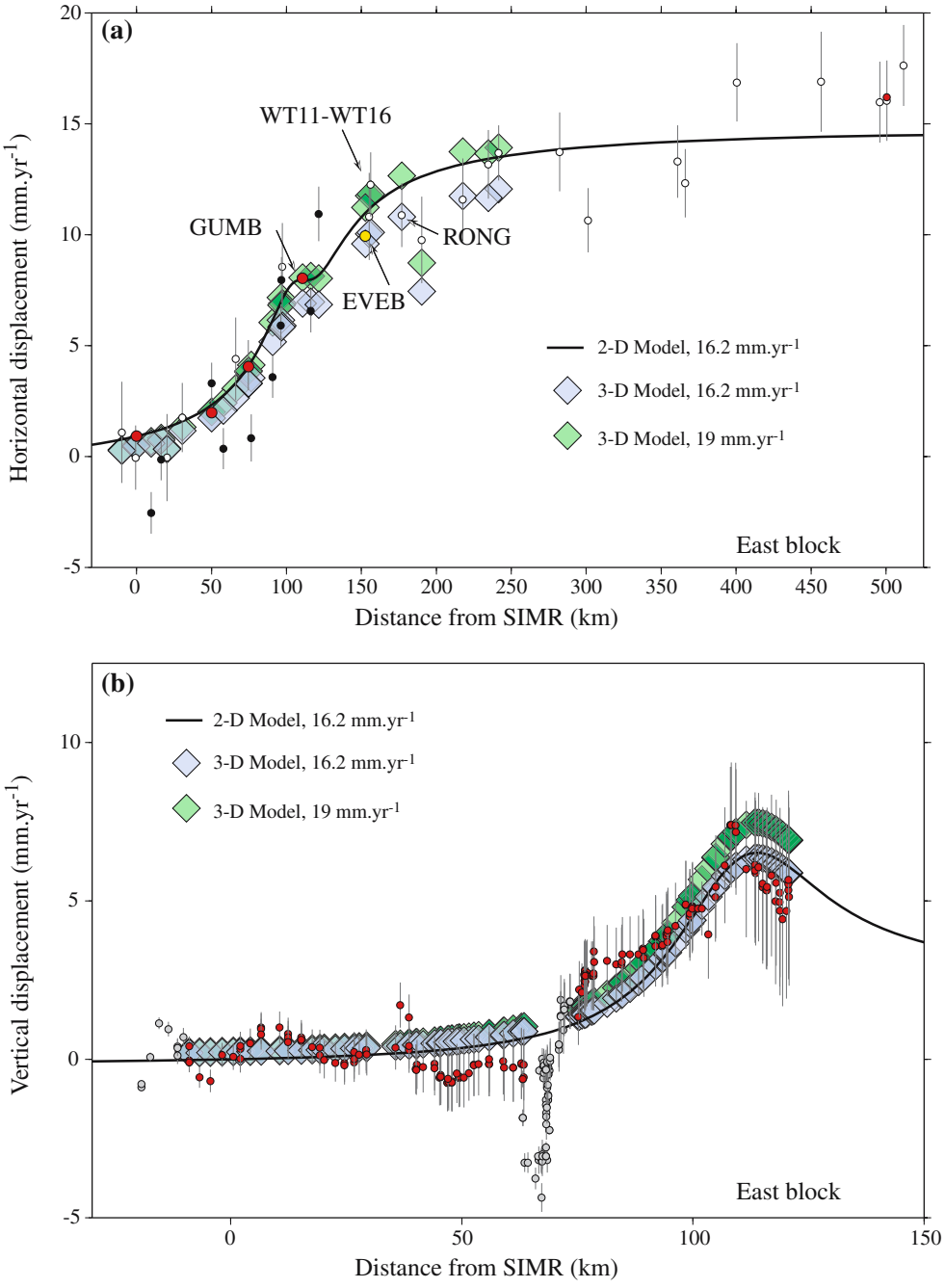

Fig. 12 **a** Horizontal velocities across the Himalaya of Central and Eastern Nepal projected on an N23°E cross-section (AA' in Fig. 10) for the Central and Eastern Nepal. *Red dots* cGPS stations. *Yellow dot* DORIS station at EVEB. *Black dots* campaign GPS measurements. *White dots* velocities determined after Chen et al. (2004). The *continuous black* line shows prediction from a model of interseismic strain computed from a creeping dislocation embedded in an elastic half-space. *Blue and green diamonds* show, respectively, prediction of a 3D point-source dislocation model (Okada 1992) for a slip rate of 16.2 and 19 mm yr^{-1}. Data around Lhasa, quite far to the east of our study area, have not been taken into account. **b** Observed (Jackson and Bilham 1994) (*red dots*) and modelled (same colour code as in Fig. 12a) vertical displacements along the levelling profile across Central Nepal projected along the Kathmandu section (see location in Fig. 10). *Grey dots* show data not included in our determination of the best model. These data include some levelling data clearly affected by subsidence in Kathmandu valley and some points in the lowlands. Note that the uplift deduced from the levelling has been shifted by 0.9 mm yr^{-1}, which is the mean uplift rate in the foreland

can be used jointly, but that lateral variations of the geometry of the locked fault zone would need to be taken into account. Note that in the joint inversion we did not normalise the respective uncertainties on the levelling and the GPS data to avoid putting too much weight on the levelling data, which all come from a single section. The solution best fitting all geodetic data yields a slip rate on the MHT of 16.2 ± 0.8 mm yr^{-1} (Fig. 12, Table 9).

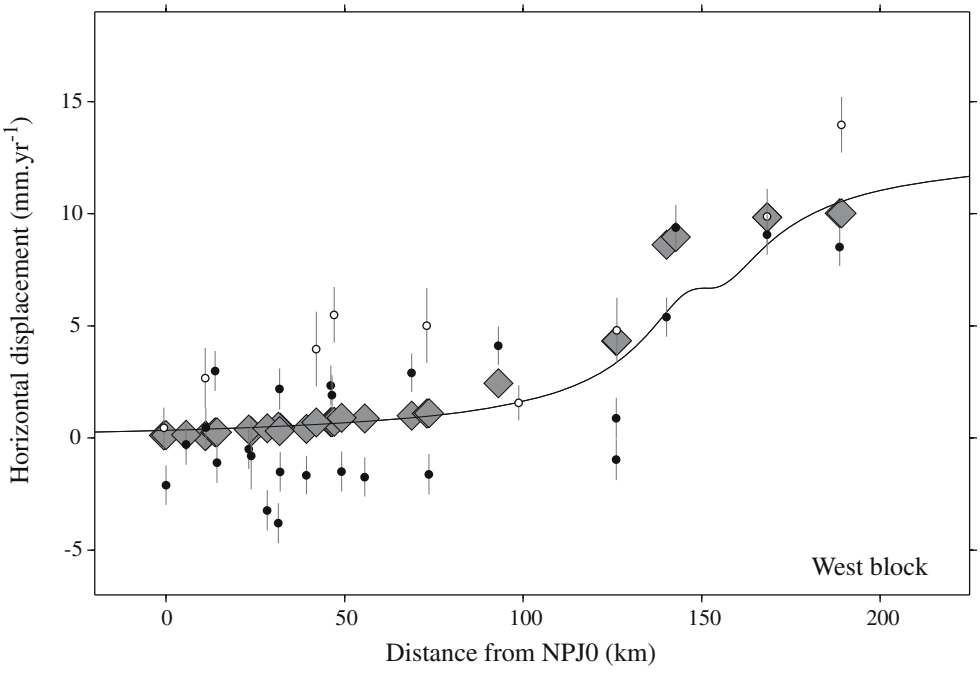

Fig. 13 Interseismic velocities across the Himalaya of Western Nepal projected on a N30°E cross section (BB' in Fig. 10). Comparison with elastic dislocation modelling (*continuous black line*) and predicted velocities determined with the revised 3D point-source dislocation model (*grey diamonds*). *Black dots* show velocities at the campaign stations determined from this study. *White dots* show velocities derived from Chen et al. (2004)

For Western Nepal, only GPS campaign measurements are available. In this region, all the data are projected along a section striking N30°E, normal to the mean azimuth of the microseismic midcrustal cluster. This velocity section shows that stations along the Himalayan foothills are approximately fixed relative to stable India and that velocities tend to increase northwards reaching 10–14 mm yr^{-1} (Fig. 13). There is obviously more scattering in these data than in the Central-Eastern Nepal section. The pattern of deformation in Western Nepal might therefore be more complex than that predicted from a simple 2D model.

The predicted velocities obtained from a purely dip-slip dislocation yield a poor fit to the N30°E velocity with a reduced χ^2 of 6.0 (Fig. 13, Table 9). The inferred slip rate is 13.4 $\pm$ 5 mm yr^{-1}, an estimate comparable with the 14 $\pm$ 1 mm yr^{-1} convergence rate determined further west across the Kumaon Himalaya in India (Banerjee and Burgmann 2002). However, compared with our analysis we suspect that, given the limited data used by Banerjee and Burgmann (2002), the 1 mm yr^{-1} uncertainty has been underestimated.

In both the Western and Central-Eastern Nepal cases, the up-dip limit of the dislocation coincides with the cluster of seismicity that can be traced all along the front of the Himalayan arc (Pandey et al. 1999). This correlation is consistent with the micro-earthquakes being triggered by stress accumulation at the tip of the creeping zone (Cattin and Avouac 2000; Pandey et al. 1995). Furthermore, the location and dip-angle of the dislocation, which are well constrained in the Central-Eastern Nepal model, is found to be reasonably consistent with the proposed geometry of the MHT as imaged from the Himalayan-Nepal Tibet Seismic Experiment (HIMNT), as well as the International DEep Profiling of Tibet and the Himalaya (INDEPTH) experiments further East (Schulte-Pelkum et al. 2005; Nelson et al. 1996) (Fig. 2). The 2D models for Western and Eastern-Central Nepal do not take into account the displacements perpendicular to assumed convergence azimuth. When this component is taken into account, the 2D hypothesis turns out to be a poor approximation.

In order to take into account the 3D geometry and lateral variations of locking depth and convergence rates, we have constructed a revised version of the 3D model proposed by Boucher et al. (2004). This model is derived by the method of Flück et al. (1997) using the Okada (1992) formulation for point sources in an elastic half-space. We used the results of the 2D models to adjust the geometry of the down-dip end of the locked fault zone (Fig. 14). The lateral variation of convergence rates was assumed to be constant through the far Western and Central-Eastern Nepal segments, varying linearly in between. The convergence azimuth was next adjusted so as to fit the azimuth of the geodetic displacements relative to India.

Once the geometry was adjusted by trial and error, we then systematically varied the average convergence rate across Western Nepal and Central-Eastern Nepal around the values obtained from the 2D modelling. For each tested value, we determine the fit to all the geodetic data, and also separately evaluate the fit to the GPS campaign measurements on one hand and to the cGPS and DORIS data on the other hand (Fig. 15a). We also separately assessed the fit to the horizontal data and the levelling data (Fig. 15b).

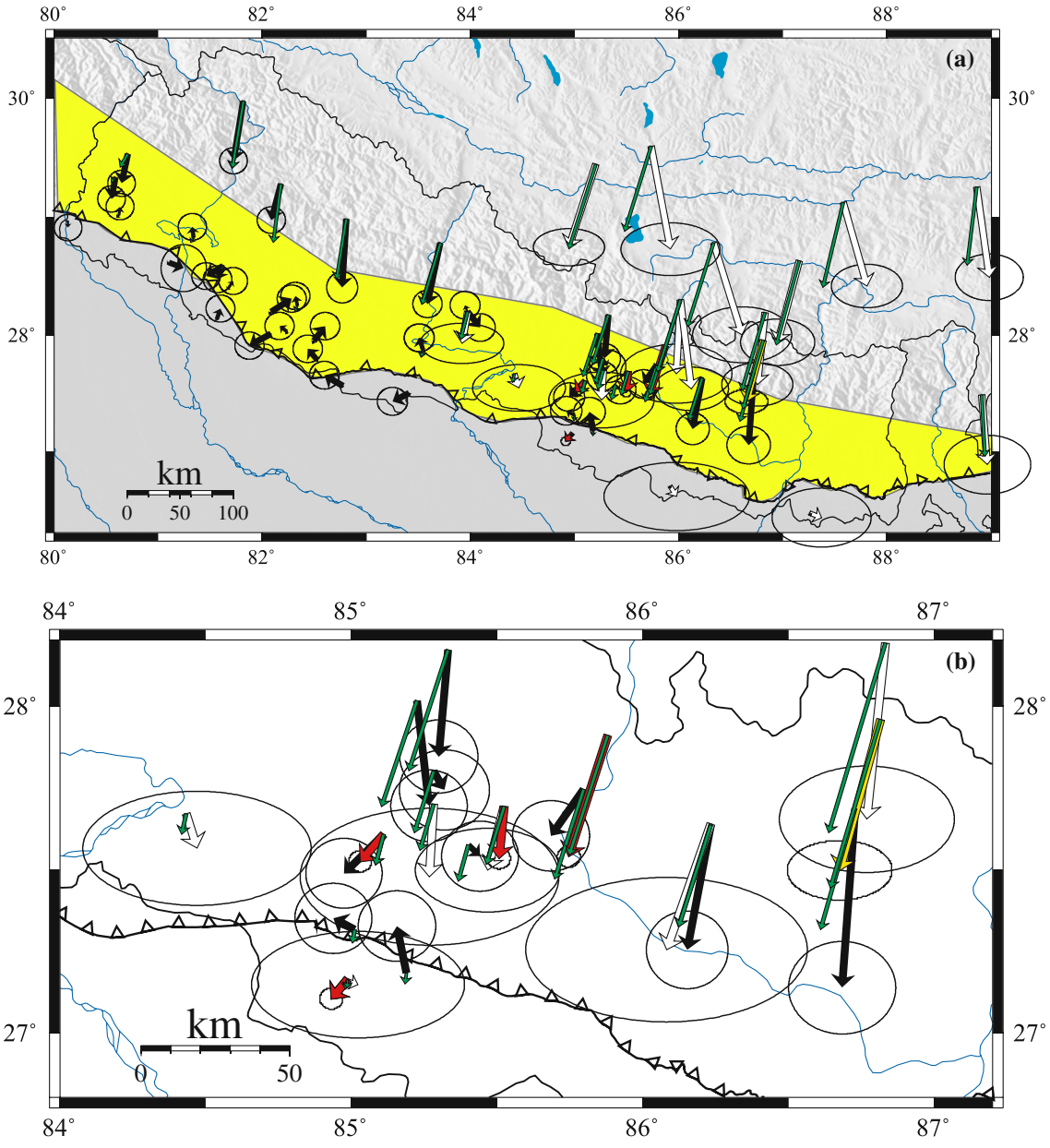

Fig. 14 **a** Observed velocities relative to stable India (same colour code as in Fig. 10) as determined in this study, and velocities predicted from a 3D point-source dislocation model (Okada 1992) (*green arrows*). Elastic moduli $\lambda = \mu = 0.33 \cdot 10^{11}\,\mathrm{Nm}^{-2}$. *Yellow area* shows the geometry of the locked fault zone of the MHT assumed in this model. Down-dip of the locked fault zone of the MHT is assumed to creep at $19\,\mathrm{mm\,yr}^{-1}$ in a direction perpendicular to the local trend of the Himalayan arc for the Central and Eastern parts and $13.4\,\mathrm{mm\,yr}^{-1}$ for the Western part. **b** Close-up view of Central and Eastern Nepal

This analysis shows that, for Central-Eastern Nepal, depending on the data set considered, the best-fitting convergence rate varies between 16 and 19 mm yr^{-1}. When all data are combined, the best-fitting shortening rate is estimated to be $19 \pm 2.5\,\mathrm{mm\,yr}^{-1}$. This model reasonably predicts the two components of horizontal displacements, as well as vertical displacements with a reduced χ^2 of 2.04. This model is more powerful than the 2D models described above in adjusting the ranges of the perpendicular and parallel displacement rates. The predicted velocities are shown in Figs. 12 and 13 in cross sections, and in Fig. 14 in plan view.

This particular solution yields an Euler pole describing the Indian plate motion relative to ITRF2000, located at $51.409 \pm 0.3°$N, $-11.415 \pm 0.5°$W, with an angular velocity of $0.480 \pm 0.015°.\mathrm{Myr}^{-1}$. This is nearly identical to the value obtained in Sect. 4, although with a smaller uncertainty (given again at the 67% confidence level). In Fig. 16, we show an azimuthal plot of residual horizontal velocities at all

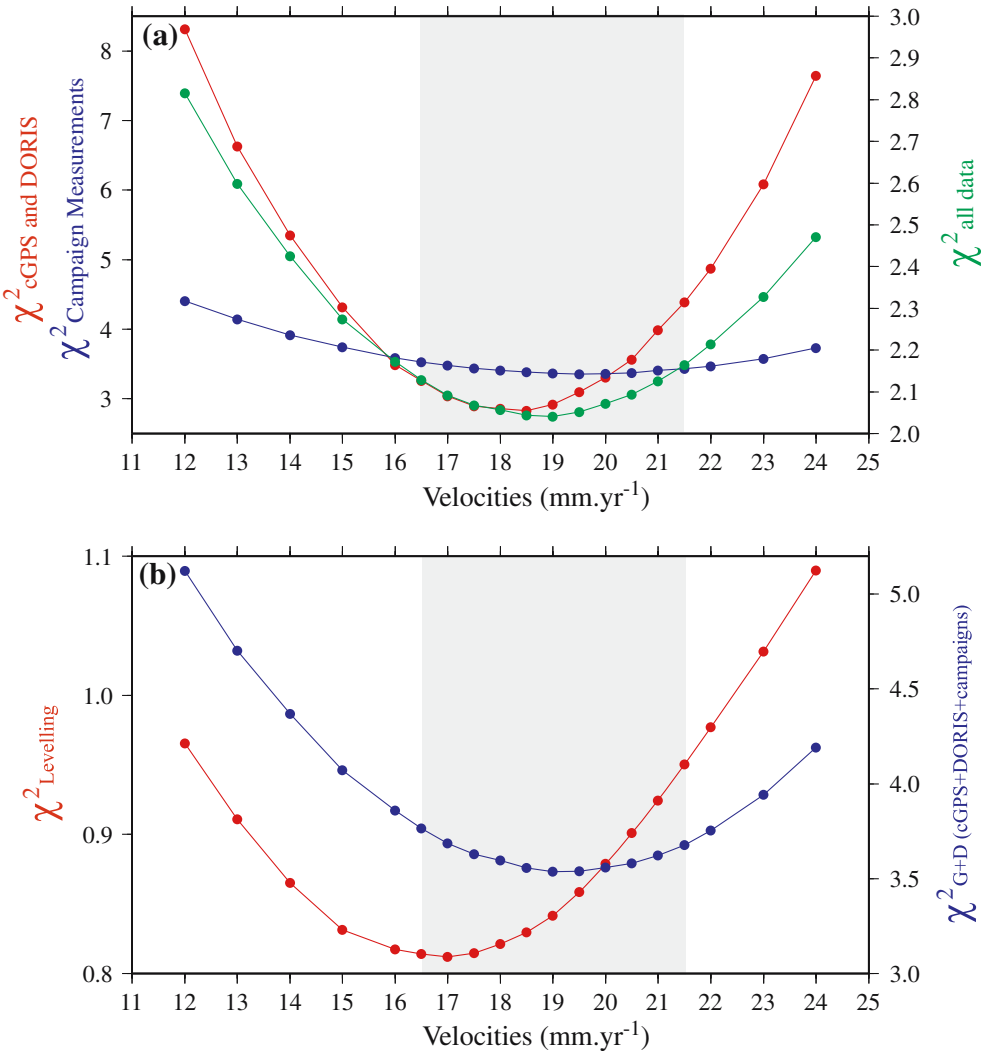

Fig. 15 Normalised reduced χ^2 as a function of slip rate. **a** *Blue and red dots* represent, respectively, the reduced χ^2 calculated from the campaign data and the cGPS–DORIS. *Green dots* show both the GPS–DORIS and levelling data. **b** *Red and blue dots* represent, respectively, the reduced χ^2 calculated from the levelling data and all the horizontal velocities

stations on the Indian plate or across the Nepal Himalaya. There is no systematic pattern here, suggesting that 3D effects are reasonably well taken into account and that our estimate of the shortening rate is not biased by the solution found for the Indian plate motion.

The four main contributors to the misfit are the predicted velocities at the permanent GPS stations NAGA, DAMA, GUMB, SIMR, and the DORIS station EVEB. It seems that the data around Everest suggest a slower convergence rate than farther west (Fig. 12). More precisely, velocities at EVEB and GUMB are better adjusted by the 16.2 and 19 mm yr^{-1} solutions, respectively. On the basis of these differences, as well as because the campaign stations nearby in Southern Tibet, i.e. RONG ($V_{N023} = 11.2$ mm yr^{-1}) and WT11/WT16 ($V_{N023} = 12.1$ mm yr^{-1}) tend to confirm these trends (cf. Fig. 12), small ($< 20\%$) lateral variations of slip rates along strike in Central-Eastern Nepal might be inferred. Given that we were not convinced of the real significance of this difference, we have not tried to complicate the model.

Based on the 2D and 3D models discussed above, we estimate the convergence rate across the Eastern and Central Himalaya to 19 mm yr^{-1}. Using the 1-σ confidence interval, and taking into account the uncertainty in the geometry of the model, the interseismic strain is estimated to be in the range 16.5–21.5 mm yr^{-1}.

6 Discussion and conclusion

In this study, we have successfully combined geodetic data from campaign GPS surveys, cGPS stations and DORIS stations to determine the plate motion of India and contemporary crustal strain across Nepal Himalaya. We were able to derive a relatively well-constrained Euler pole to describe the motion of India relative to ITRF2000. We infer very little internal deformation of India, with deformation rates less than 1.8 mm yr^{-1} based on the baseline change between SIMR and IISC.

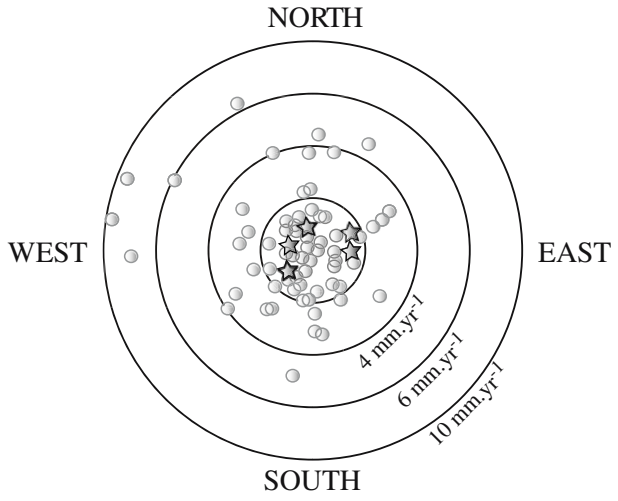

Fig. 16 Azimuthal plot of residual horizontal velocities, relative to the best-fitting 3D model corresponding to Fig. 15, at all stations located either on the Indian Plate or across the Nepal Himalaya. As in Fig. 9, stars show stations that were used to determine the Euler pole of India in Table 7

The pattern of crustal deformation across the Eastern and Central Himalaya, also documented from levelling data, implies that the MHT is locked over a distance of about 115 km from the surface to a depth of about 20 km beneath the front of the mountain range. Horizontal shortening due to ductile creep along the deeper portion of the MHT appears to fall in the range 16.5–21.5 mm yr^{-1} along strike in Central and Eastern Nepal. Small ($< 20\%$ of the slip rate) lateral variations are suspected in that area but are not properly resolved due to the low spatial sampling of the area.

These rates are consistent with, but better constrained than, previous geodetic estimates, and it now becomes clearer that the geodetic rate might be slightly lower than the geological slip determined at 21.5 ± 1.5 mm yr^{-1} for the Holocene period in that region (Lavé and Avouac 2000). This lower slip rate might imply that postseismic relaxation, which must follow large earthquakes, in the region is now well over. The last large earthquake along that portion of the Himalaya is the Bihar–Nepal Mw 8.0–8.2 earthquake, which occurred in 1934. The Maxwell time in this context, i.e. the characteristic time associated with viscous relaxation (Cohen 1999), is thus probably significantly smaller than about 60 years.

Across Western Nepal, the pattern of deformation and the shortening rate, given to be around 13.4 ± 5 mm yr^{-1}, is less well constrained due to the lack of cGPS stations. The width of the locked fault zone seems somewhat larger in this area. The apparently lower shortening rate there (than across Eastern and Central Nepal) might be related to the even longer time span since the last large earthquake in this area. This observation will be useful to assess the mechanical properties of the crust and lithosphere and stress variations during the seismic cycle.

Acknowledgements We are grateful to Jeff Freymueller and two anonymous reviewers for most helpful suggestions and comments, and to Will Featherstone for his careful editorial review of the manuscript. We also thank Jeff Genrich for useful comments and suggestions. We are most grateful to all the people who have contributed to the data acquisition, in particular M. Thankauri, B. Chaudhary, B. Kaffle (DMG, Kathmandu); J.B. De Chabalier (Institut de Physique du Globe de Paris (IPGP)), J. Lavé (Laboratoire de Géophysique Interne et de Tectonophysique (LGIT)), R. Cattin (Ecole Normale Supérieure (ENS)). T. Héritier, J. Rouault, and S. Carré, all at Commissariat à l'Energie Atomique/Département Analyse Surveillance Environnement (CEA/DASE), have greatly contributed to this project. We thank Roger Bilham for making available the GPS campaign data collected by him and his colleagues at the Cooperative Institute for Research in Environmental Sciences (CIRES, University of Colorado). This study benefited also from the GPS campaign data collected during the Centre National de la Recherche Scientifique/Institut National des Sciences de l'Univers (CNRS/INSU) program IDYL-HIM. The realisation of the DORIS time-series was carried out at the Jet Propulsion Laboratory (JPL) under a contract with the National Aeronautics and Space Administration (NASA). This work was supported by the CEA, the CNRS IDYL-Him project and the Betty and Gordon Moore Foundation. This is Caltech Tectonics Observatory contribution number 32. The maps in this paper were generated using the public-domain Generic Mapping Tools (GMT) software (Wessel and Smith 2001).

References

Altamimi Z, Sillard P, Boucher C (2002) ITRF2000: a new release of the international terrestrial reference frame for Earth science applications. J Geophys Res – Solid Earth 107(B10):2214, DOI: 10.1029/2001JB000561

Argus, DF, Gordon RG (1991) No-net-rotation model of current plate velocities incorporating plate motion model nuvel-1. Geophys Res Lett 18(11):2039–2042, DOI: 10.1029/91GL01532

Avouac JP (2003) Mountain building, erosion and the seismic cycle in the Nepal Himalaya. In: Advances in geophysics 46. Dmowska R (ed), Elsevier, Amsterdam, pp 1–80, DOI:10.1016/S0065-2687(03)46001-9

Avouac JP, Bollinger L, Lavé J, Cattin R, Flouzat M (2001) Le cycle sismique en Himalaya. C. R. Acad Sci 333:513–529

Banerjee P, Burgmann R (2002) Convergence across the northwest Himalaya from GPS measurements. Geophys Res Lett 29(13) art. no.-1652, DOI:10.1029/2002GL015184

Beutler G, Rothacher M, Schaer S, Springer TA, Kouba J, Neilan RE (1999) The International GPS Service (IGS), An interdisciplinary service in support of earth sciences. Adv Space Res 23(4):631–653

Beutler, G, Bock H, Brockmann E, Dach R, Fridez P, Gurtner W, Hugentobler U, Ineichen D, Johnson J, Meindl M, Mervart L, Rothacher M, Schaer S, Springer T, Weber R (2001) Bernese GPS Software, Version 4.2. Astronomical Institute, University of Berne, Berne

Beutler G, Drewes H, Verdun A (2005) The Integrated Global Geodetic Observing System (IGGOS) viewed from the perspective of history. J Geodyn 40(4–5):414–431, DOI: 10.1016/j.jog.2005.06.005

Bilham R, Larson K, Freymueller J, Jouanne F, LeFort P, Leturmy P, Mugnier JL, Gamond JF, Glot JP, Martinod J, Chaudury NL, Chitrakar GR, Gautam UP, Koirala BP, Pandey MR, Ranabhat R, Sapkota SN, Shrestha PL, Thakuri MC, Timilsina UR, Tiwari DR, Vidal G, Vigny C, Galy A, deVoogd B (1997) GPS measurements of present-day convergence across the Nepal Himalaya. Nature 386(6620):61–64, DOI: 10.1038/386061a0

Bilham R, Blume F, Bendick R, Gaur VK (1998) Geodetic constraints on the translation and deformation of India: Implications for future great Himalayan earthquakes. Curr Sci 74(3):213–229

Blewitt G, Bock Y, Kouba J (1995) Constructing the IGS polyhedron by distributed processing. In Proc. of the IGS Workshop ed. By J. Zumberge, IGS Central Bureau, Pasadena, pp 31–36

Bollinger L, Avouac JP, Cattin R, Pandey MR (2004) Stress buildup in the Himalaya. J Geophys Res 109(B11):B11405, DOI: 10.129/2003JB002911

Boucher C, Altamimi Z, Sillard P (1999) The 1997 International Terrestrial Reference Frame (ITRF97). IERS Techn. Note 27, Paris Observatory

Boucher C, Altamimi Z, Sillard P, Feissel-Vernier M (2004) The International Terrestrial Reference Frame (ITRF2000). IERS Tech Note 31 Verlag des Bundesamts fur Kartographie und Geodasie, Frankfurt am Main

Cattin R, Avouac JP (2000) Modeling mountain building and the seismic cycle in the Himalaya of Nepal. J Geophys Res 105(B6):13389–13407, DOI: 10.1029/2000JB900032

Chen Z, Burchfiel BC, Liu Y, King RW, Royden LH, Tang W, Wang E, Zhao J, Zhang X (2000) Global Positioning System measurements from eastern Tibet and their implications for India/Eurasia intercontinental deformation. J Geophys Res 105:16215–16227, DOI: 10.1029/2000JB900092

Chen QZ, Freymueller JT, Wang Q, Yang ZQ, Xu CJ, Liu JN (2004) A deforming block model for the present-day tectonics of Tibet. J Geophys Res 109(B1):art. no.-B01403, DOI:10.1029/2002JB002151

Cohen SC (1999) Numerical models of crustal deformation in seismic zones. Adv Geophys (41):133–231

Crétaux JF, Soudarin L, Cazenave A, Bouille F (1998) Present-day tectonic plate motions and crustal deformations from the DORIS space system. J Geophys Res 103(B12):30167–30181

DeMets C, Gordon RG, Argus DF, Stein S (1994) Effect of recent revisions to the geomagnetic reversal time scale on current plate motions. Geophys Res Lett 21:2191–2194

Dong D, Herring TA, King RW (1998) Estimating regional deformation from a combination of space and terrestrial geodetic data. J Geod 72(4):200–214

Flouzat M, Avouac JP, Durette B, Bollinger L, Heritier T, Jouanne F, Pandey M (2002) Interseismic deformation across the Himalaya of Central Nepal from GPS measurements. EOS Trans AGU 83(47) Fall Meet Suppl F366

Flück P, Hyndman RD, Wang K (1997) Three-dimensional dislocation model for great earthquakes of the Cascadia subduction zone. J Geophys Res 102(B9):20539–20550

Gahalaut VK, Chander R (1997) On interseismic elevation changes and strain accumulation for great thrust earthquakes in the Nepal Himalaya. Geophys Res Lett 24:1011–1014

Hauck ML, Nelson D, Brown LD, Zhao W, Ross AR (1998) Crustal structure of the Himalayan orogen at 90° east longitude from Project INDEPTH deep reflection profiles. Tectonics 17:481–500

Holt WE, Chamot-Rooke N, Le Pichon X, Haines AJ, Shen-Tu B, Ren J (2000) Velocity field in Asia inferred from Quaternary fault slip rates and Global Positioning System observations. J Geophys Res 105:19185– 19209, DOI: 10.1029/2000JB900045

Jackson M., Bilham R (1994) Constraints on Himalayan deformation inferred from vertical velocity fields in Nepal and Tibet. J Geophys Res 99(B7):13897–13912

Jouanne F, Mugnier JL, Pandey M, Gamond JF, Le Fort P, Serrurier P, Vigny C, Avouac JP, IDYL-HIM members. (1999) Oblique convergence in Himalaya of western Nepal deduced from preliminary results of GPS measurements. Geophys Res Lett 26(13):1933–1936

Jouanne F, Mugnier JL, Gamond JF, Le Fort P, Pandey MR, Bollinger L, Flouzat M, Avouac JP (2004) Current shortening across the Himalayas of Nepal. Geophys J Int 157(1):1–14, DOI: 10.1111/j.1365-246X.2004.02180.x

Kreemer C, Haines J, Holt WE, Blewitt G, Lavalee D (2000) On the determination of a global strain rate model. Earth Planets Space 52:765–770

Kumar S, Wesnousky SG, Rockwell TK, Ragona D, Thakur VC, Seitz GG (2001) Earthquake recurrence and rupture dynamics of Himalayan Frontal Thrust, India. Science 294(5550):2328–2331

Larson K, Bürgmann R, Bilham R, Freymueller JT (1999) Kinematics of the India-Eurasia collision zone from GPS measurements. J Geophys Res 104(B1):1077–1093

Lavé J, Avouac JP (2000) Active folding of fluvial terraces across the Siwaliks Hills, Himalayas of central Nepal. J Geophys Res 105(B3):5735–5770

Lavé J, Yule D, Sapkota S, Basant K, Madden C, Attal M, Pandey R (2005) Evidence for a great medieval earthquake (approximate to 1100 AD) in the Central Himalayas, Nepal. Science 307(5713):1302–1305, DOI:10.1126/science.1104804

Melbourne WG (1985) The case for ranging in gps based geodetic system. In: Proceedings of the 1st international symposium on precise positioning with the global positioning system, Clyde Goad (ed), pp 373–386

Mervart L (1995) Ambiguity Resolution Techniques in Geodetic and Geodynamic Applications of the Global Positioning System. Geodätisch-geophysikalische Arbeiten in der Schweiz, Band 53 Schweizerische Geodätische Kommission Institut für Geodäsie und Photogrammetrie Eidg. Technische Hochschule Zürich

Molnar P, Pandey MR (1989) Rupture zones of great earthquakes of the Himalayan region. Indian Acad Sci (Earth and Planetary Science) 98(1):61–70

Nelson KD, Zhao WJ, Brown LD, Kuo J, Che JK, Liu XW, Klemperer SL, Makovsky Y, Meissner R, Mechie J, Kind R, Wenzel F, Ni J, Nabelek J, Chen LS, Tan HD, Wei WB, Jones AG, Booker J, Unsworth M, Kidd WSF, Hauck M, Alsdorf D, Ross A, Cogan M, Wu CD, Sandvol E, Edwards M (1996) Partially molten middle crust beneath southern Tibet: Synthesis of project INDEPTH results. Science 274(5293):1684–1688

Okada Y (1992) Internal deformation due to shear and tensile fault in a half space. Bull Seismol Soc Am 82:1018–1040

Paul J, Bürgmann R, Gaur VK, Bilham R, Larson KM, Ananda MB, Jade S, Mukal M, Anupama TS, Satyal G, Kumar D (2001) The motion and active deformation of India. Geophys Res Lett 28:647–650, DOI: 10.1029/2000GL011832

Pandey MR, Tandukar RP, Avouac JP, Lave J, Massot JP (1995) Interseismic Strain Accumulation on the Himalayan Crustal Ramp (Nepal). Geophys Res Lett 22(7):751–754

Pandey MR, Tandukar RP, Avouac JP, Vergne J, Héritier T (1999) Seismotectonics of Nepal himalayas from a local seismic network. J Asian Earth Sci 17(5–6):703–712

Perfettini H, Avouac JP (2004) Stress transfer and strain rate variations during the seismic cycle. J Geophys Res 109(B2):B02304, DOI: 10.1029/2003JB002917

Press WH, Teukolsky SA, Vetterling WT, Flannery BP (1992) Numerical Recipes, The Art of Scientific Computing. (Second Edition) Cambridge University Press, Cambridge, ISBN 0-521-43108-5

Ray J, Dong D, Altamimi Z (2004) IGS reference frames: status and future improvements. GPS Solutions 8(4):251–266, DOI: 10.1007/s10291-004-0110-x

Schulte-Pelkum V, Monsalve G, Sheehan A, Pandey MR, Sapkota S, Bilham R, Wu F. (2005) Imaging the Indian subcontinent beneath the Himalaya. Nature 435 (7046):1222–1225, DOI: 10.1038/nature03678

Sella GF, Dixon TH, Mao AL (2002) REVEL: A model for recent plate velocities from space geodesy. J Geophys Res 107(B4), DOI: 10.1029/2000JB000033

Shen ZK, Zhao C, Yin A, Li Y, Jackson DD, Fang P, Dong D (2000) Contemporary crustal deformation in east Asia constrained by Global Positioning System measurements. J Geophys Res 105(B3):5721–5734

Singh SJ, Rani S (1993) Crustal deformation associated with two-dimensional thrust faulting. J Phys Earth 41(2) 87–101

Sillard P, Altamimi Z, Boucher C (1998) The ITRF96 realization and its associated velocity field. Geophys Res Lett 25(17):3223–3226

Socquet A (2003) Accommodation du mouvement relatif entre l'Inde et la Sonde: depuis la Faille de Sagaing jusqu'à la Syntaxe Est Himalayenne. Thèse de doctorat de l'Université Paris XI, 195 pp

Soudarin L, Cretaux JF, Cazenave A (1999) Vertical crustal motions from the DORIS space-geodesy system. Geophys Res Lett 26(9):1207–1210

Tapley BD, Bettadpur S, Ries JC, Thompson PF, Watkins MM (2004) GRACE measurements of mass variability in the Earth system. Science 305(5683):503–505, DOI: 10.1126/science.1099192

Tavernier G, Fagard H, Feissel-Vernier M, Lemoine F, Noll C, Ries J, Soudarin L, Willis P (2005) The International DORIS Service (IDS). Adv Space Res 36(3):333–341, DOI:10.1016/j.asr.2005.03.102

Vergne J, Cattin R, Avouac JP (2001) On the use of dislocations to model interseismic strain and stress build-up at intracontinental thrust faults. Geophys J Int 147(1):155–162

Webb F, Zumberge J Eds. (1995) An introduction to the GIPSY/OASIS II, Report JPLM D-11088, Jet Propulsion Laboratory, Pasadena

Wessel P, Smith WHF (2001) The generic mapping tools (GMT) version 3.4 technical reference & cookbook. School of Ocean and Earth Science and Technology/National Oceanic and Atmospheric Administration (SOEST/NOAA)

Williams SDP, Bock Y, Fang P, Jamason P, Nikolaidis RM, Prwirodirdjo L, Miller M, Johnson DJ (2004) Error analysis of continuous GPS position time series. J Geophys Res 109(B3):B03412, DOI: 10.1029/2003JB002741

Willis P, Heflin M (2004) External validation of the GRACE GGM01C gravity field using GPS and DORIS positioning results. Geophys Res Lett 31(13):L13616, DOI: 10.1029/2004GL020038

Willis P, Ries JC (2005) Defining a DORIS core network for Jason-1 precise orbit determination based on ITRF2000; methods and realization. J Geod 79(6–7):370–378, DOI: 10.1007/s00190-005-0475-9

Willis P, Haines B, Berthias JP, Sengenes P, Le Mouel JL (2004) Behavior of the DORIS/Jason oscillator over the South Atlantic Anomaly. CR Geoscience 336(9):839–846, DOI:10.1016/j.crte.2004.01.004

Willis P, Berthias JP, Bar-Sever YE (2006) Systematic errors in the Z-geocenter derived using satellite tracking data: A case study from SPOT-4 DORIS data in 1998. J Geod, 79(10–11):567–572 DOI:10.1007/s00190-005-0013-9

Willis P, Boucher C, Fagard H, Altamimi Z (2005b) Geodetic applications of the DORIS system at the French Institut Geographique National. CR Geoscience 337(7):653–662, DOI:10.1016/j.crte.2005.03.002

Wubbena G (1985) Software Developments for Geodetic Positioning with GPS Using TI 4100 Code and Carrier Measurements. In: Proceedings of the 1st international symposium on precise positioning with the global positioning system, Clyde Goad (ed), pp 403–412

Yoshioka S, Mikumo T, Kostoglodov V, Larson KM, Lowry AR, Singh S (2004) Interplate coupling and a recent aseismic slow slip event in the Guerrero seismic gap of the Mexican subduction zone, as deduced from GPS data inversion using a Bayesian information criterion. Phys Earth Planetary Interiors 146(3–4):513–530, DOI: 10.1016/j.pepi.2004.05.006

Zhang J, Bock Y, Johnson H, Fang P, Genrich JF, Williams S, Wdowinski S, Behr J (1997) Southern California permanent GPS geodetic array: error analysis of daily position estimates and site velocities. J Geophys Res 102(18):035-18 055, DOI: 10.1029/97JB01380

Zhao W, Nelson KD, project INDEPTH Team (1993) Deep seismic-reflection evidence continental underthrusting beneath southern Tibet. Nature 366(6455):557–559